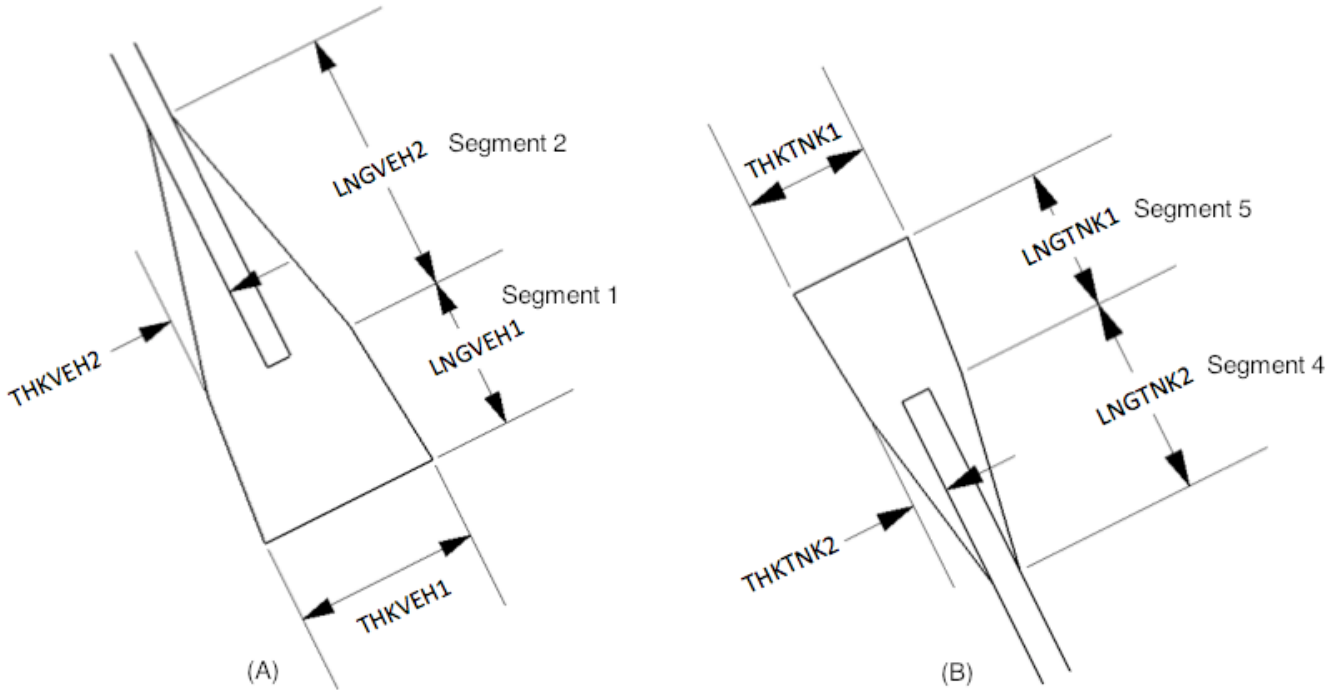


Fig. 1a Left side: **Discretized BIGBOSOR4 model of the optimized “oneskirt” tank2/skirt system** obtained with the use of the “temporary” versions of bosdec (bosdec.tank2.density.var [2]) and addbosor4 (addbosor4.tank2.density.var [2]). Right side: **Schematic of the configuration of the five-segment skirt support.** The bottom end of the skirt is simply supported to “ground” (the rigid launch vehicle). The lengths and thicknesses of the metallic parts of the skirt ends: LNGVEH1 and THKVEH1 in Segment 1, LNGVEH2 and THKVEH2 in Segment 2, LNGTNK1 and THKTNK1 in Segment 5, LNGTNK2 and THKTNK2 in Segment 4, are “decision variable candidates”. These variables are identified in the next figure and are listed and defined in Table 1. The thicknesses, THICK(i), and layup angles, ANGLE(i), of the composite plies in the wall of the skirt are also “decision variable candidates”. A “decision variable candidate” is a problem variable that has Role Type 1 as assigned by the GENOPT user and as listed in Table 1.



**Fig. 1(b) Decision variable candidates for (A) Segments 1 and 2 of the aft skirt and (B) Segments 4 and 5 of the aft skirt.** In the “twoskirt” case there are two skirts, an aft skirt and a forward skirt. The forward skirt slants outward with increasing meridional distance along the reference surface, as shown in Fig. 8a, instead of inward with increasing meridional distance along the reference surface, as shown here. What are called “Segment 1” and “Segment 2” of the aft skirt in (A) above become, respectively, “Segment 5” and “Segment 4” of the forward skirt, and what are called “Segment 4” and “Segment 5” of the aft skirt in (B) above become, respectively, “Segment 2” and “Segment 1” of the forward skirt. As seen from Table 1, the variables, LNGVEH1, THKVEH1, LNGVEH2, THKVEH2, LNGTNK1, THKTNK1, LNGTNK2, THKTNK2, are arrays with dimension 2. The first element in the arrays, THKVEH1(1) and THKVEH2(1), etc. corresponds to the aft skirt, and the second element in the arrays, THKVEH1(2) and THKVEH2(2), etc. corresponds to the forward skirt. Notice that the thicknesses of the metallic (isotropic) “prongs” in Segments 2 and 4 are tapered and that the thicknesses of the metallic (isotropic) Segments 1 and 5 are also tapered. This tapering is included in the GENOPT/BIGBOSOR4 models. In STAGS models of these conical skirt segments the corresponding thicknesses are constant and equal to the average thicknesses of the tapered parts. This approximation is made in the STAGS models in order to avoid the need for the introduction of user-written subroutines.

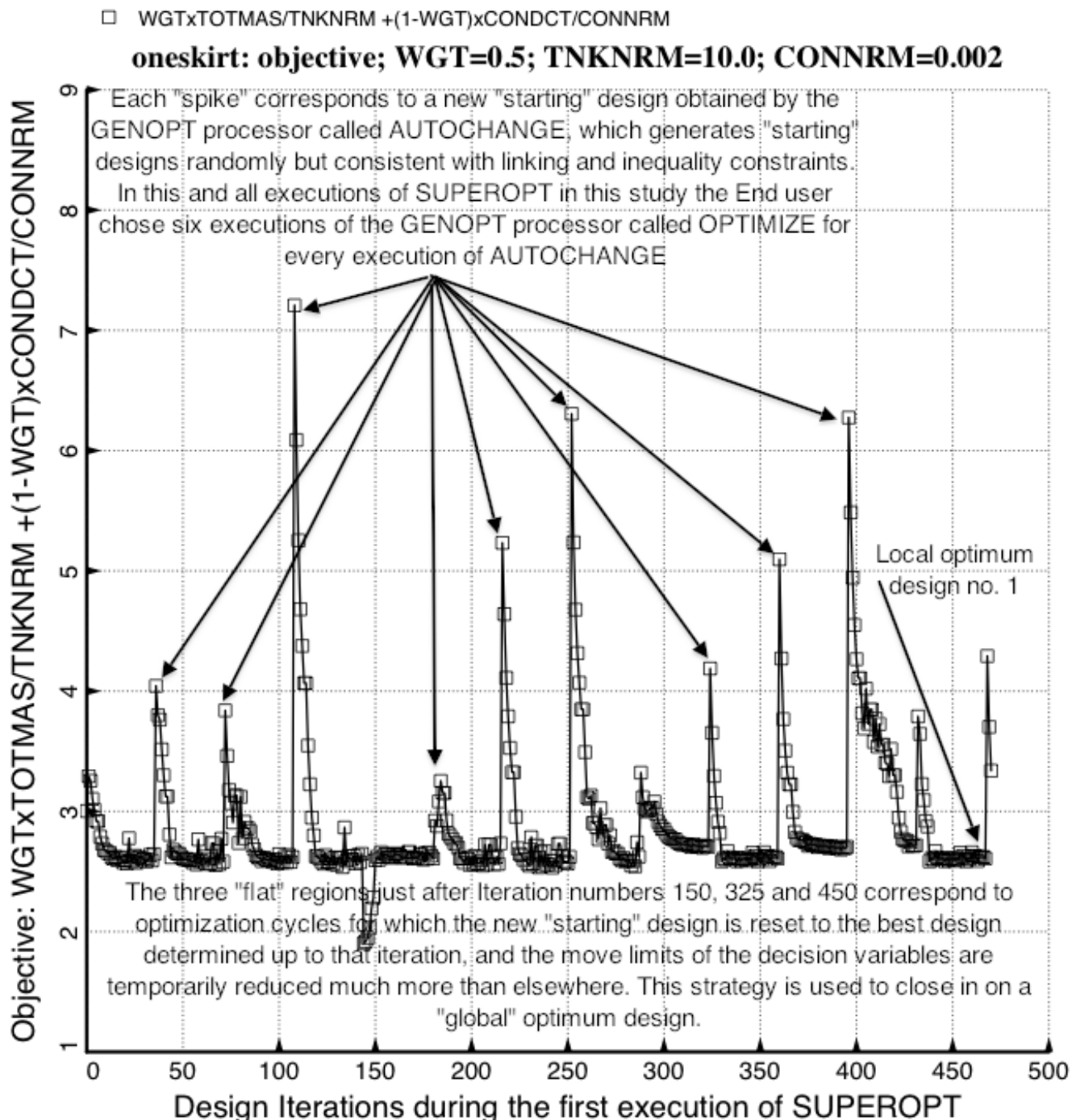


Fig. 2 Results from the specific case called “oneskirt”: Optimization of the long propellant tank with one skirt connected to the midlength of the cylindrical part of the propellant tank. (See Fig. 1a.) The starting design at the beginning of the second execution of SUPEROPT (next figure) is the same as that labeled here as: “Local optimum design no. 1”. The quantities, WGT, TNKNRM and CONNRM, are specified by the End user in the GENOPT processor called “BEGIN” (Table 2). The units of TNKNRM and CONNRM are lb-sec<sup>2</sup>/inch and BTU/hr-deg.R, respectively.

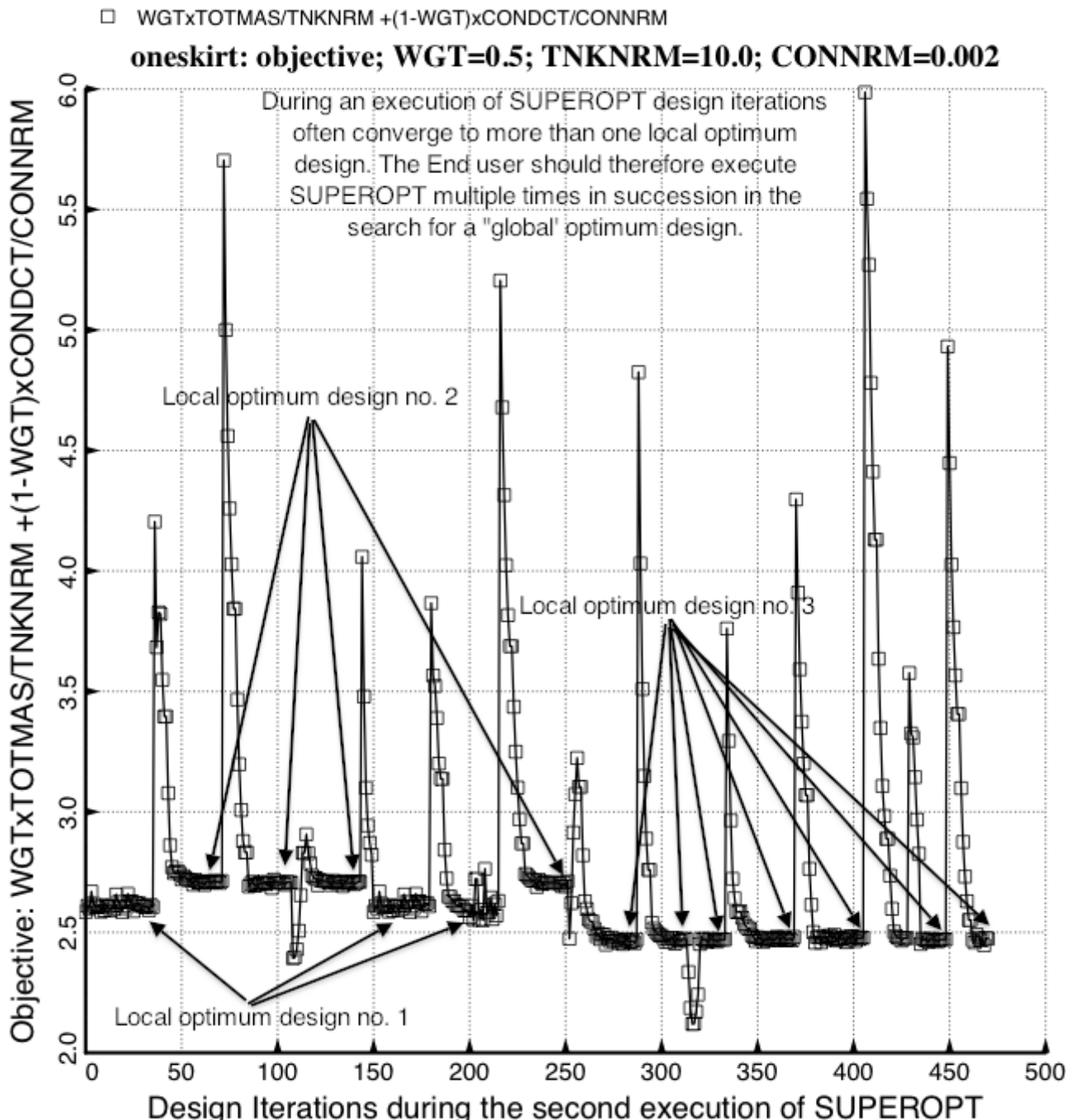
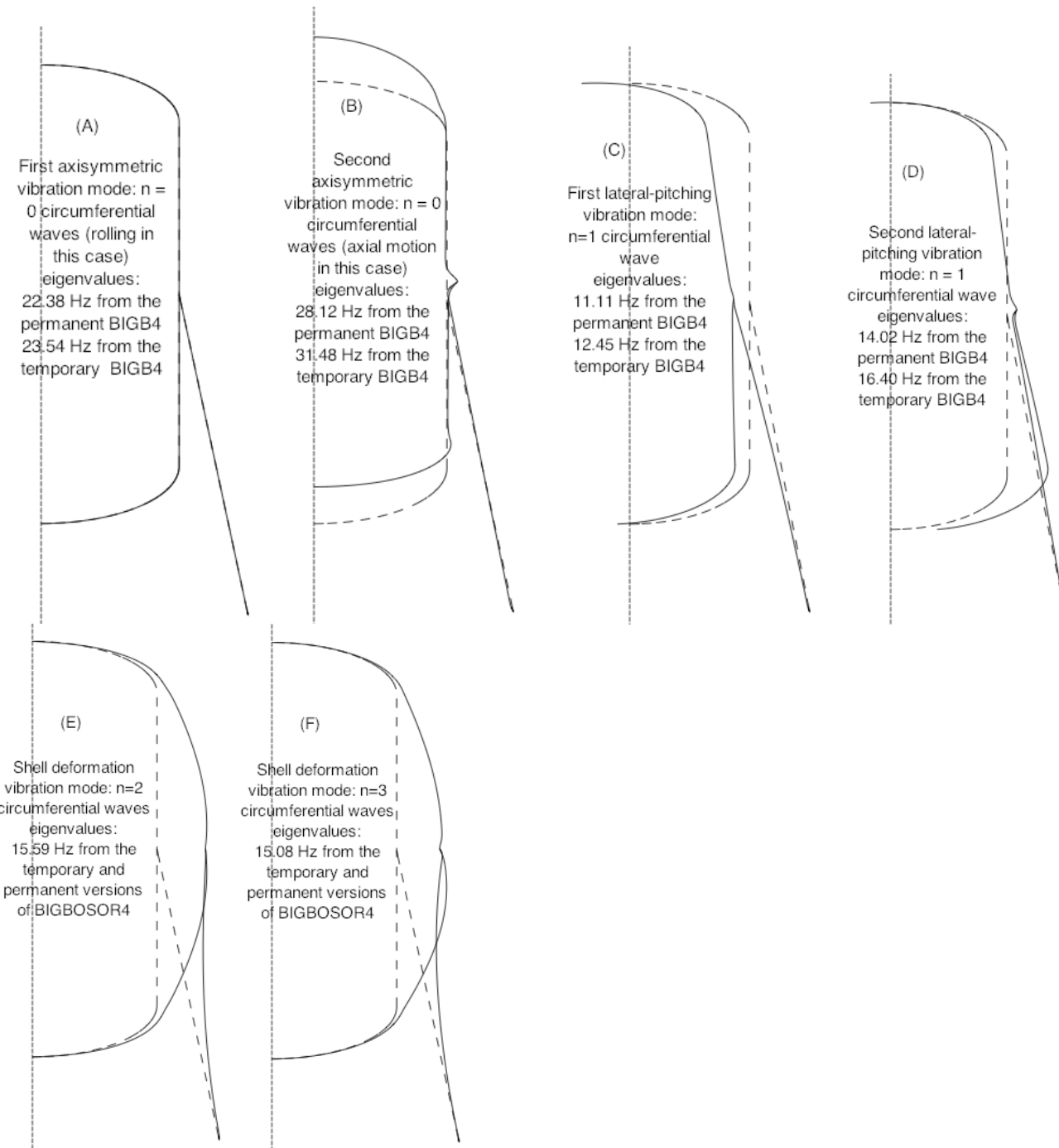
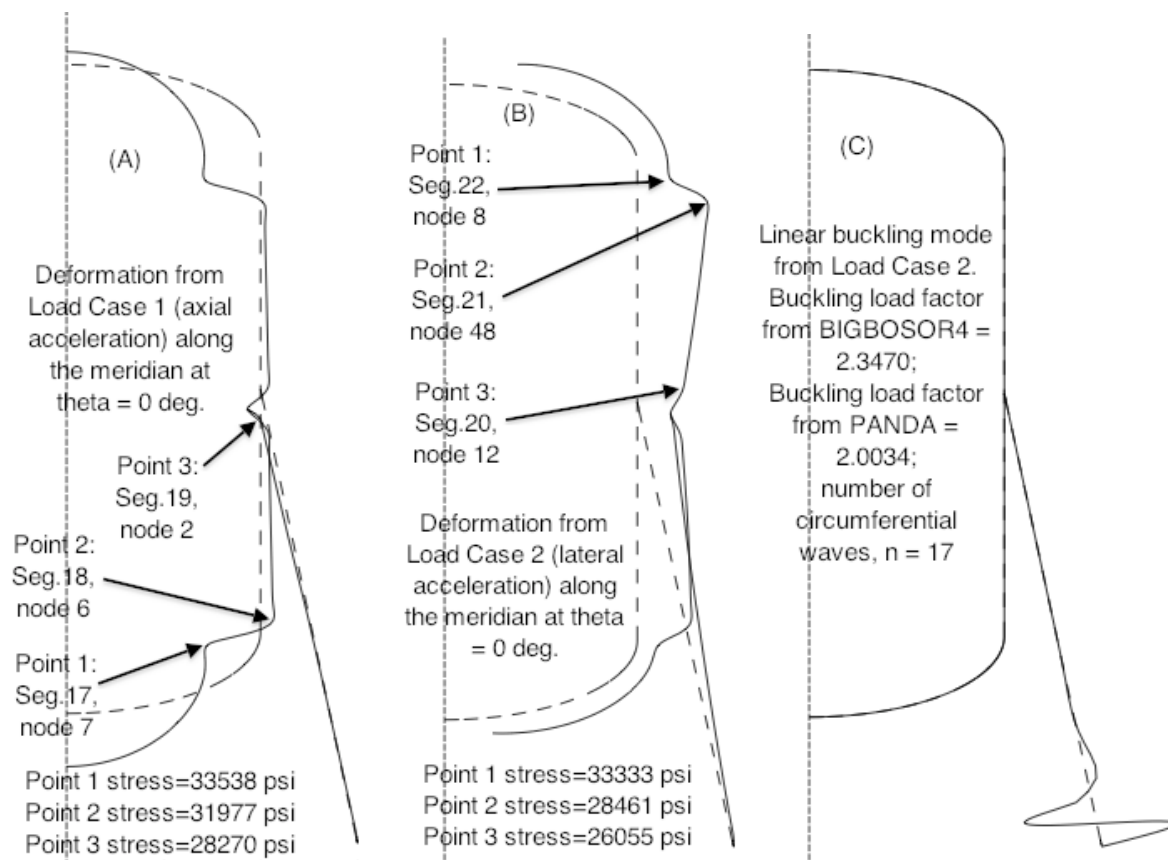


Fig. 3 Results from the specific case called “oneskirt”: Further optimization of the long propellant tank with one skirt connected to the midlength of the cylindrical part of the propellant tank. The starting design at the beginning of this second execution of SUPEROPT is the same as that labeled, “Local optimum design no. 1” in the previous figure. Notice that there is more than one local optimum design. This behavior makes it difficult to determine the “global” optimum design, usually calling for multiple successive executions of SUPEROPT in order to come close to the “global” optimum design.



**Fig. 4 Vibration modes from GENOPT/BIGBOSOR4 for the optimized propellant tank with one skirt attached at the midlength of the cylindrical part of the tank.** “permanent BIGB4” means the stand-alone version of BIGBOSOR4, for which the lumped density of the propellant is constant along the meridian of each shell segment of the propellant tank (bosdec.tank2 and addbosor4.regular [2]). “temporary BIGB4” means the temporarily modified version of BIGBOSOR4, for which the lumped density of the propellant may vary within each shell segment of the propellant tank (bosdec.tank2.density.var and addbosor4.tank2.density.var [2]). The temporarily modified version of BIGBOSOR4 yields somewhat higher frequencies than the permanent version of BIGBOSOR4 because there is more mass in the end domes in the permanent model, and this mass is farther from the axis of revolution, producing higher rolling inertia and higher lateral/pitching inertia.



**Fig. 5 Prebuckled states, (A), (B) and a buckling mode (C) from GENOPT/BIGBOSOR4 for the optimized propellant tank with one skirt attached at the midlength of the cylindrical part of the tank.** The stress values in (A) and (B) are taken from Table 3. In (A) the stress at Point 1 is fiber tension at the tips of the internal orthogrid stringers (layer 1) in the aft ellipsoidal dome near its equator (Segment 17, node 7, layer 1,  $z = -0.49$  inch); the stress at Point 2 is the outer surface effective stress in the skin near the aft end of the cylindrical part of the tank (Segment 18, node 6, layer 2,  $z = +0.03$  inch); and the stress at Point 3 is the outer surface effective stress adjacent to the thin end of the tapered external doubler (Segment 19, node 2, layer 3,  $z = +0.03$  inch). In (B) the stress at Point 1 is fiber tension at the tips of the internal orthogrid stringers (layer 1) in the forward ellipsoidal dome near its equator (Segment 22, node 8, layer 1,  $z = -0.44$  inch); the stress at Point 2 is the outer surface effective stress in the skin (layer 2) near the junction of the cylindrical part of the tank with the forward ellipsoidal dome (Segment 21, node 48, layer 2,  $z = +0.03$  inch); and the stress at Point 3 is the outer surface effective stress adjacent to the thin end of the upper half of the tapered external doubler (Segment 20, node 12, layer 3,  $z = +0.03$  inch). (C) shows the critical buckling mode shape and buckling load factors for Load Case 2 (10g lateral acceleration) corresponding to the prebuckled state along the meridian at circumferential coordinate, theta = 0 degrees. In the BIGBOSOR4 model prebuckling in-plane shear, shell wall anisotropy, and transverse shear deformation (t.s.d.) are neglected. In the approximate PANDA-type model [4] prebuckling in-plane shear, shell wall anisotropy and t.s.d. are included in an approximate model in which segment 3 of the conical skirt is modeled as an “equivalent” cylindrical shell. Note that (C) does not show the critical (lowest) buckling load factor under Load Case 2. That critical value, 1.3294, corresponds to shear buckling at theta=90 degrees, obtained from an approximate PANDA-type model as listed in Section 4.

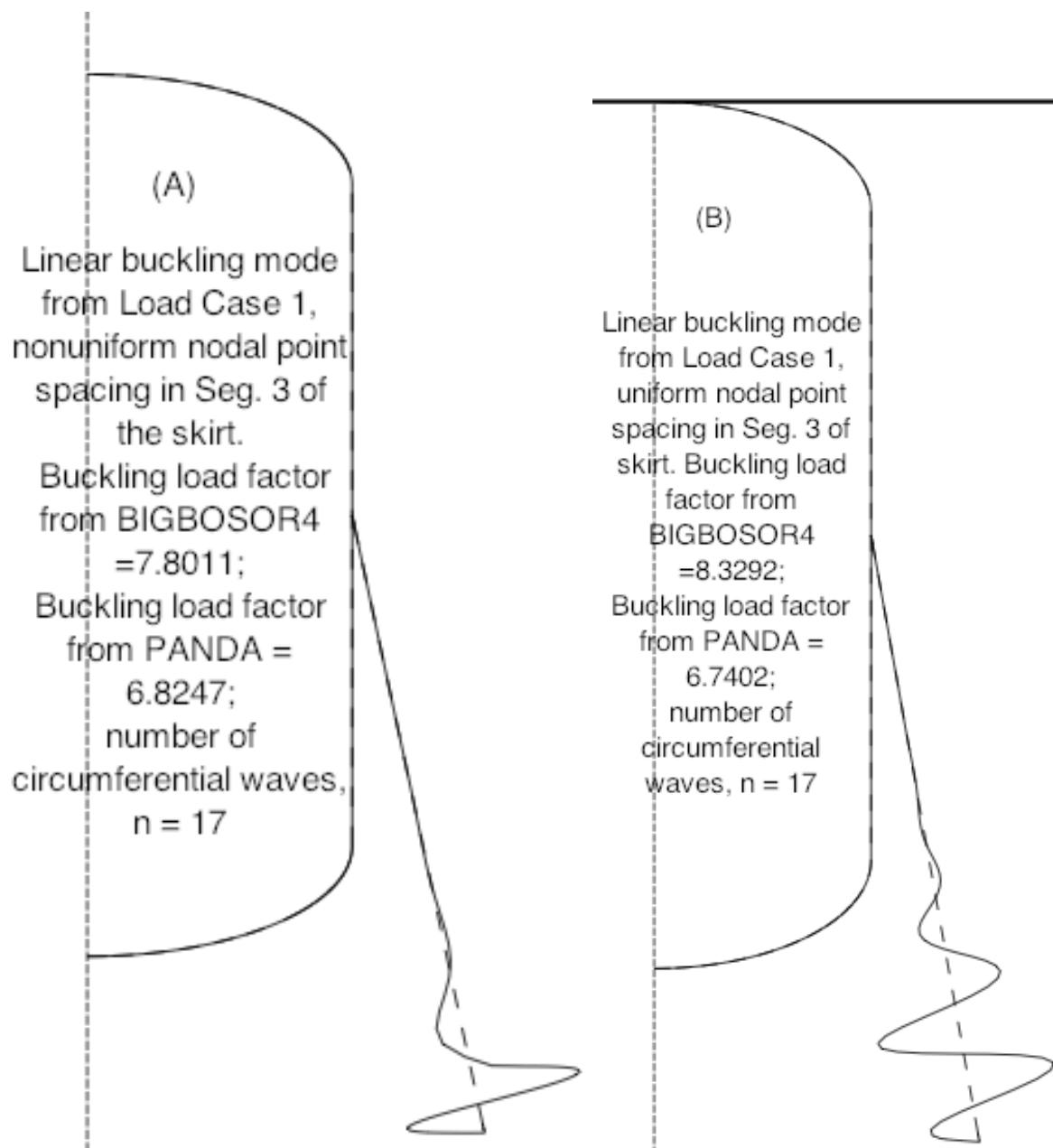


**Fig 6 Load Case 1: Comparison of buckling load factors from GENOPT/BIGBOSOR4 for linear bifurcation buckling of the skirt with (A) nonuniform nodal point spacing in Segment 3 of the skirt as shown in Fig. 1a and (B) uniform nodal point spacing in Segment 3 of the skirt.** In the GENOPT/BIGBOSOR4 software (SUBROUTINE BOSDEC [2]) the nonuniform nodal point spacing in Segment 3 of the skirt is the “standard model” (left hand side of Fig. 1a). SUBROUTINE BOSDEC was modified only temporarily for the purpose of obtaining the GENOPT/BIGBOSOR4 results shown in (B). In the BIGBOSOR4 model prebuckling in-plane shear, shell wall anisotropy, and transverse shear deformation (t.s.d.) are neglected. In the approximate PANDA-type model [4] prebuckling in-plane shear, shell wall anisotropy and t.s.d. are included in an approximate model in which segment 3 of the conical skirt is modeled as an “equivalent” cylindrical shell.

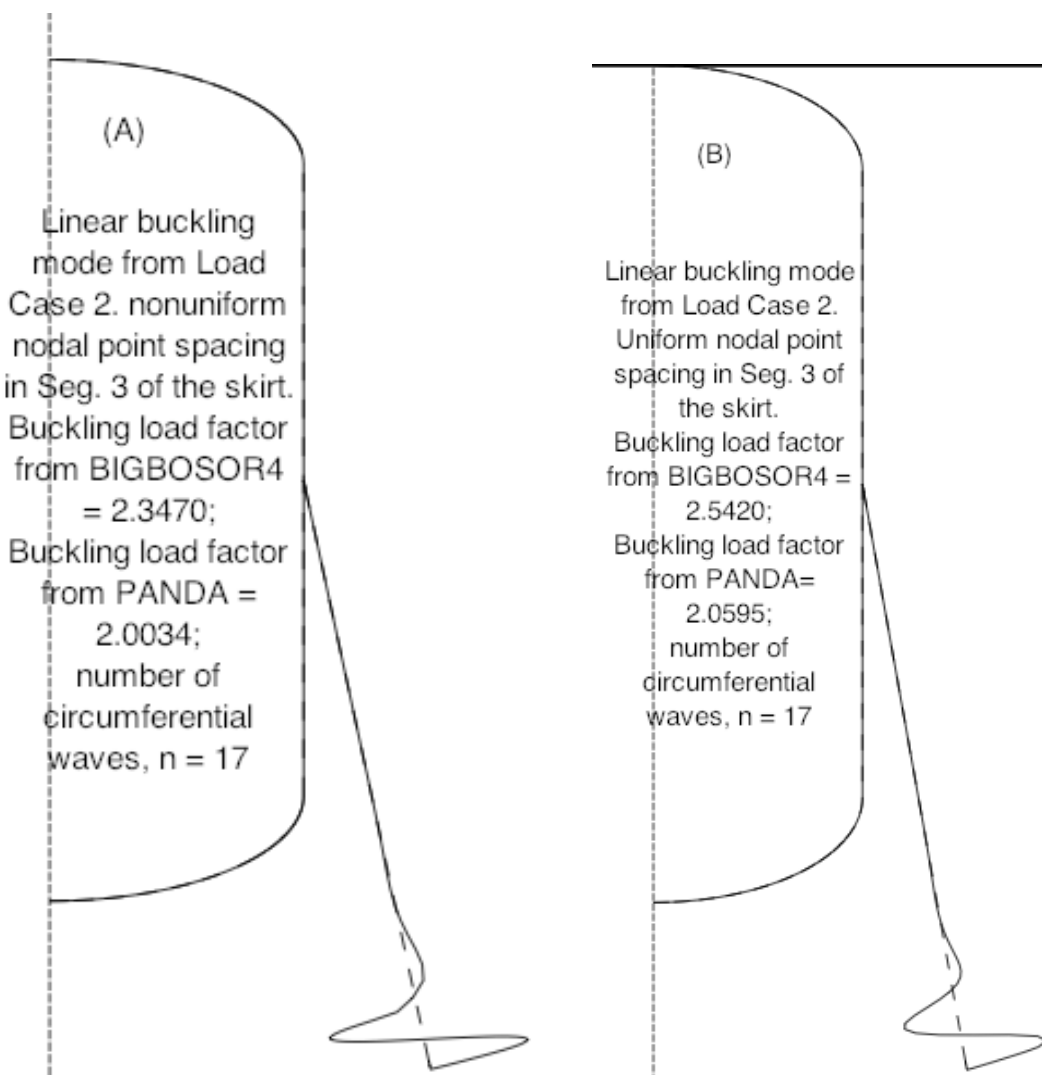


**Fig 7 Load Case 2: Comparison of buckling load factors from GENOPT/BIGBOSOR4 for linear bifurcation buckling of the skirt as loaded with the prebuckled state along the meridian at circumferential coordinate,  $\theta = 0$  degrees, with (A) nonuniform nodal point spacing in Segment 3 of the skirt and (B) uniform nodal point spacing in Segment 3 of the skirt.** In the GENOPT/BIGBOSOR4 software (SUBROUTINE BOSDEC [2]) the nonuniform nodal point spacing in Segment 3 of the skirt is the “standard model” (left-hand side of Fig. 1a). SUBROUTINE BOSDEC was modified only temporarily for the purpose of obtaining the GENOPT/BIGBOSOR4 results shown in (B). Notice that in this case the BIGBOSOR4 prediction of the buckling load factor in (A) is somewhat lower than that in (B). In the BIGBOSOR4 model prebuckling in-plane shear, shell wall anisotropy, and transverse shear deformation (t.s.d.) are neglected. In the approximate PANDA-type model [4] prebuckling in-plane shear, shell wall anisotropy and t.s.d. are included in an approximate model in which segment 3 of the conical skirt is modeled as an “equivalent” cylindrical shell.

**NOTE: The lowest (most critical) buckling mode and load factor from Load Case 2, not shown in this figure, corresponds to shear buckling at circumferential coordinate,  $\theta = 90$  degrees.** This most critical buckling mode and load factor are computed from the approximate PANDA-type model as described in Section 4. The shear buckling load factor as computed by the “PANDA” branch of GENOPT/TANK is equal to 1.3294.

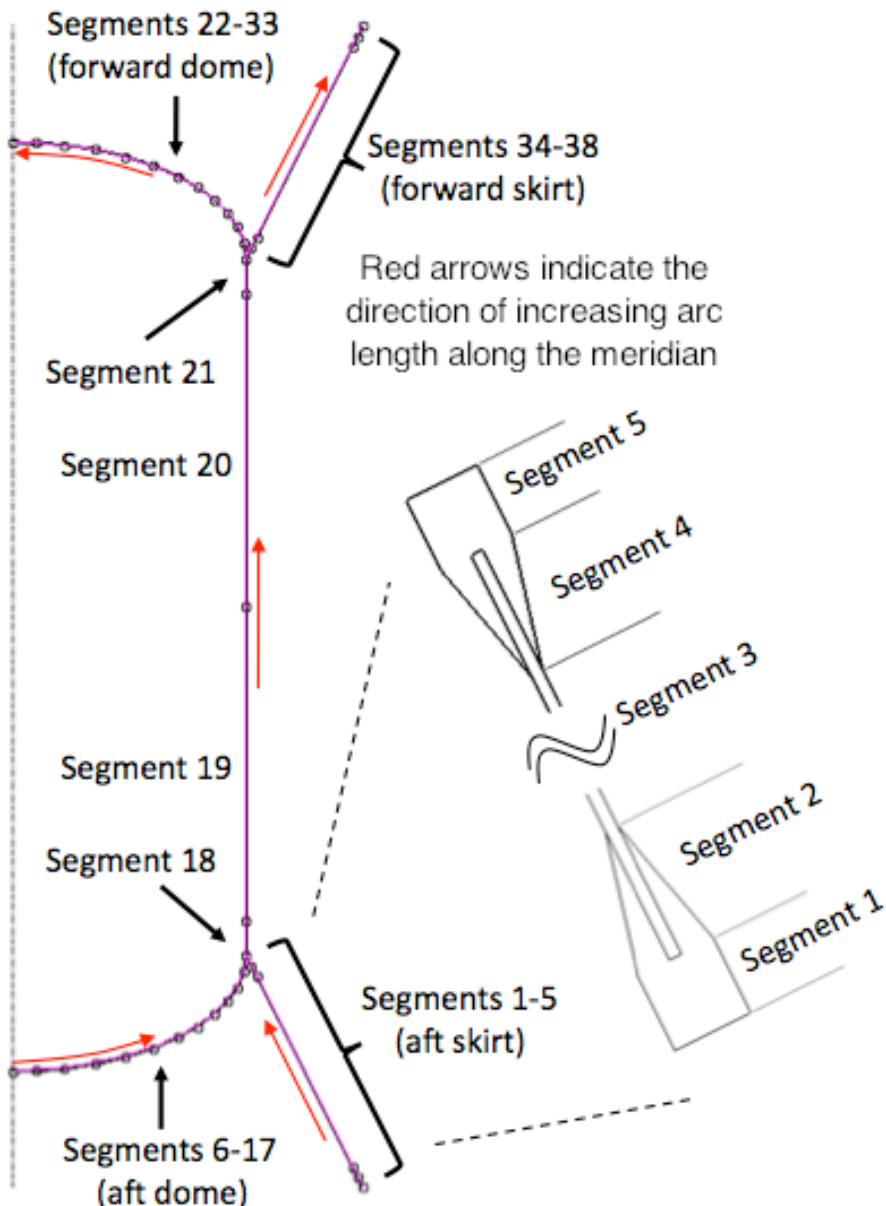


Fig. 8a **BIGBOSOR4 “twoskirt” model.** This “twoskirt” model contains 38 shell segments. The points shown here lie on the shell reference surfaces. These points indicate **only the end points of each shell segment** in the model. Each shell segment contains many nodal points, as follows: 13 nodal points in each of Segments 1, 2, 4, 5, 6 – 17, 18, 21, 22 – 33, 34, 35, 37 and 38; 53 nodal points in Segments 19 and 20 (long cylindrical segments of the propellant tank); and 99 nodal points in Segments 3 and 36 (longest segments of the laminated composite aft and forward conical skirts). **NOTE: In all the STAGS models, each part with tapered thickness in the GENOPT/BIGBOSOR4 model, such as external doublers and the four end segments of each conical skirt, are replaced by the corresponding part with constant thickness equal to half the maximum thickness of the tapered part. This is done to avoid the need for STAGS user-written subroutines.**

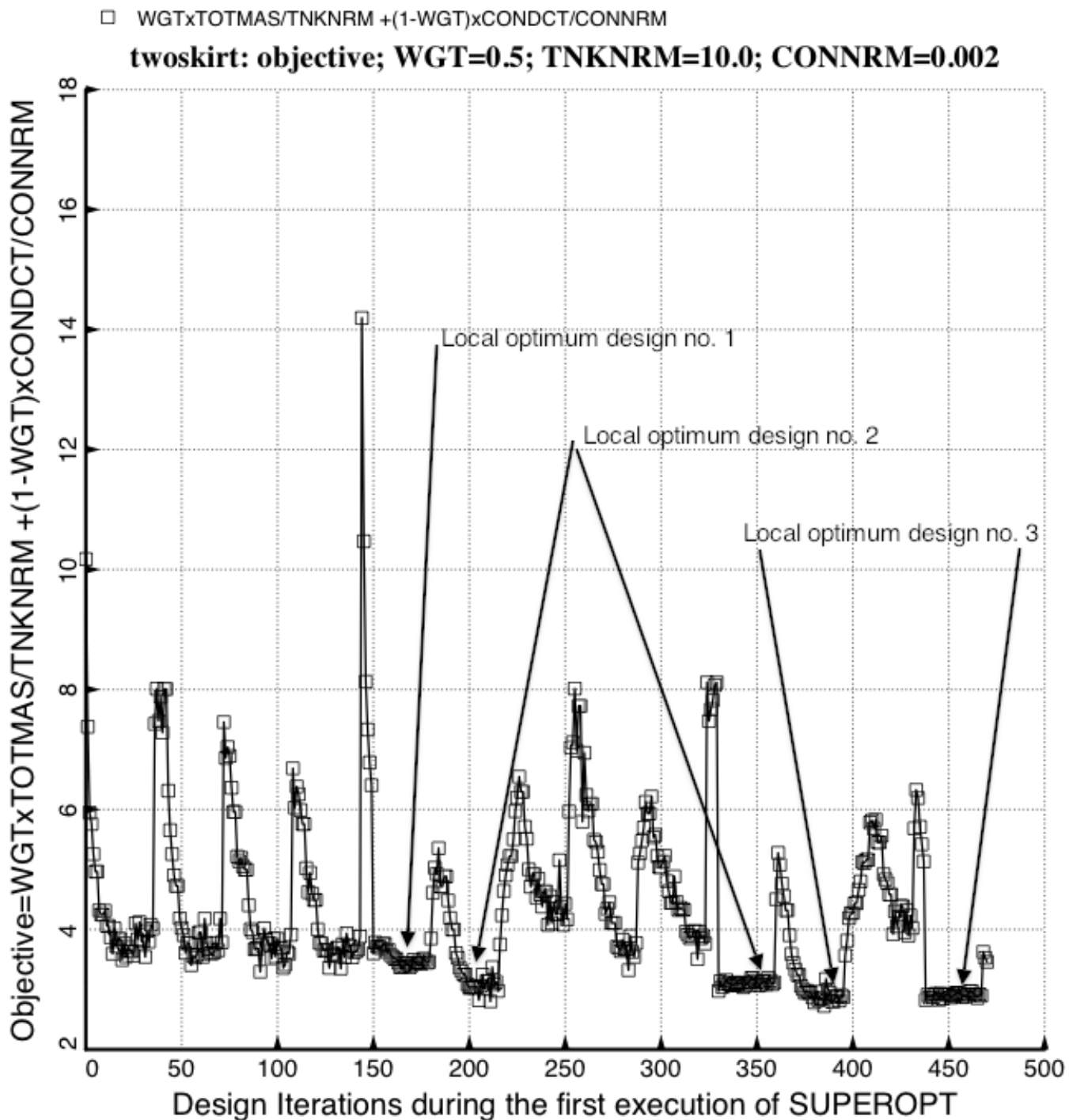
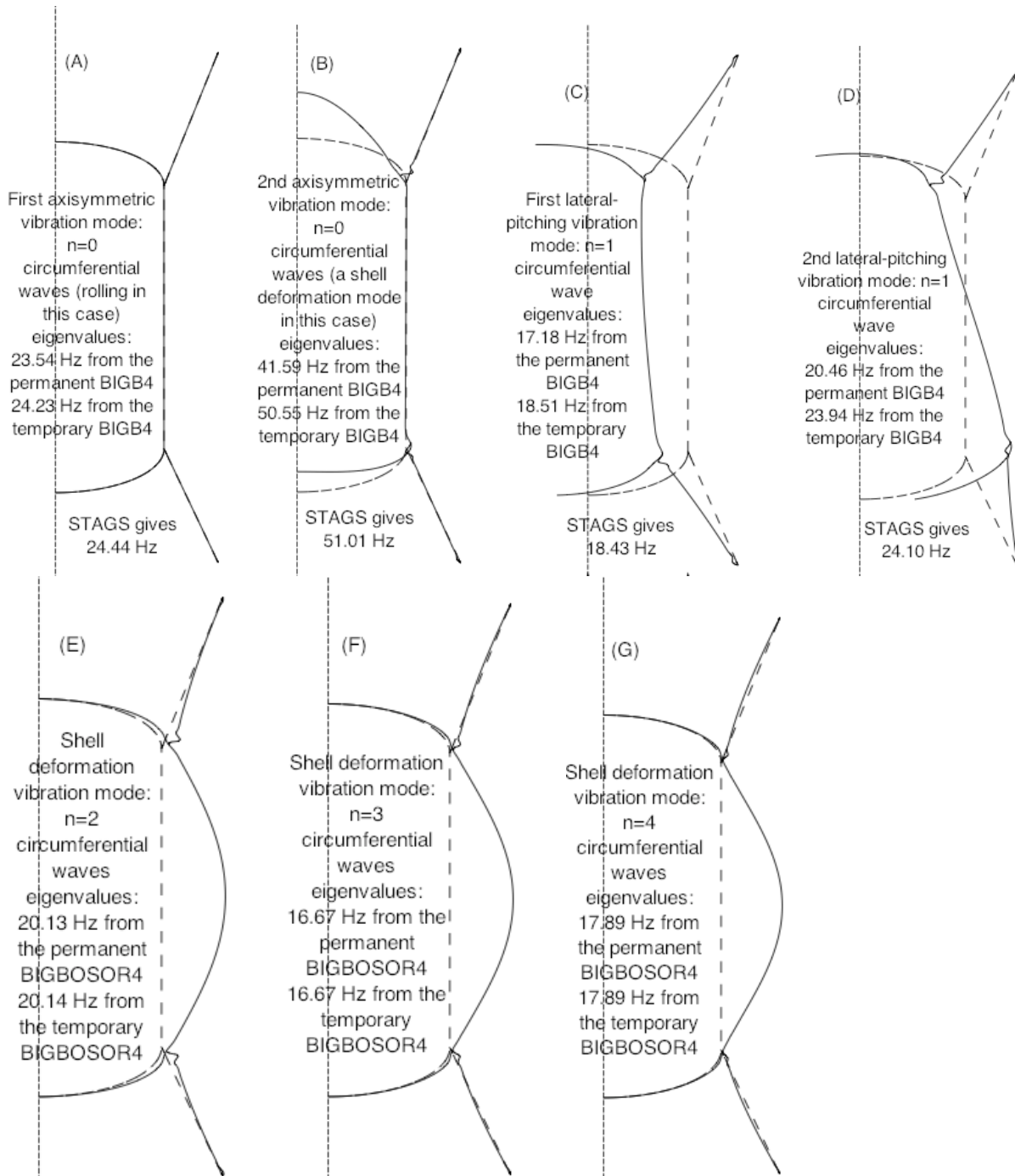
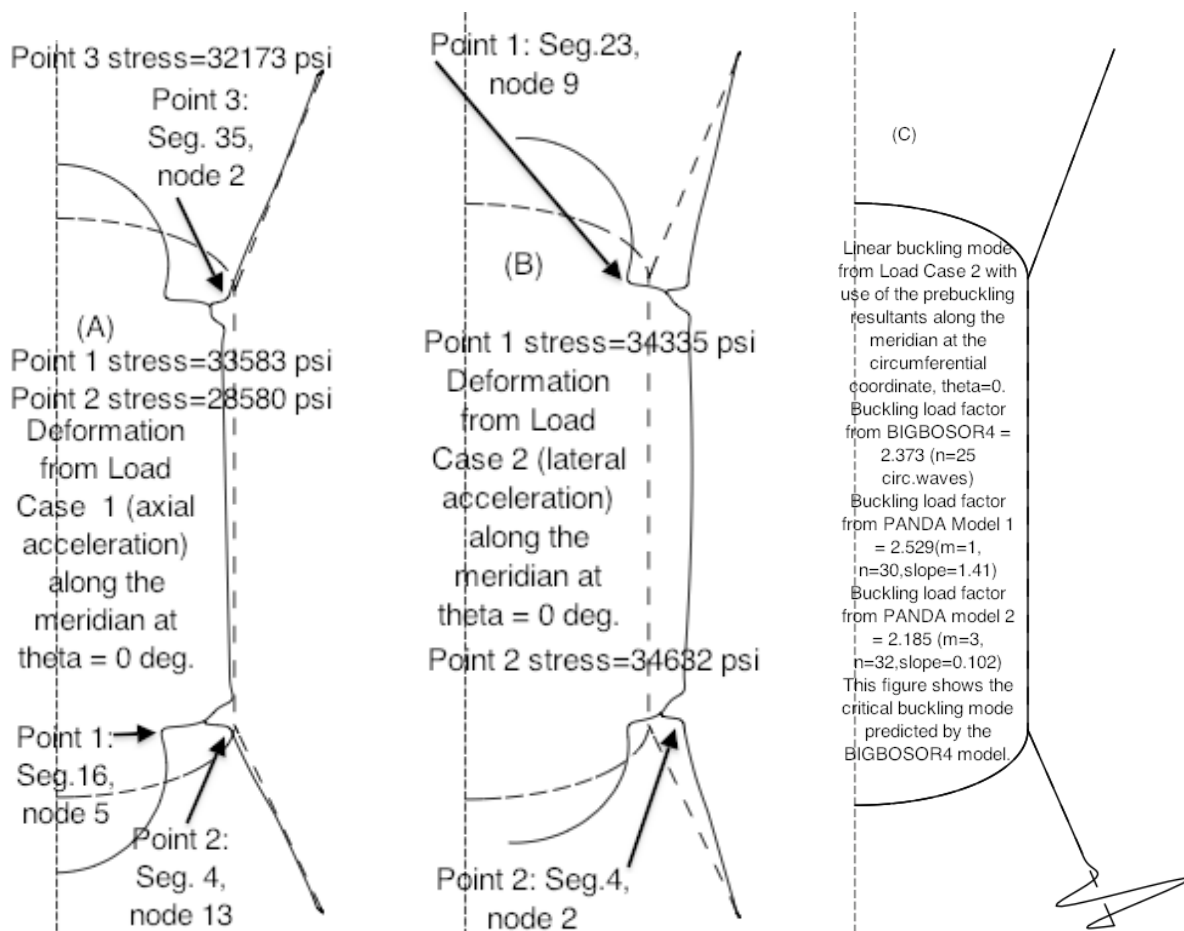


Fig. 8b **Results from the specific case called “twoskirt”:** Optimization of the long propellant tank with skirts connected to the aft and forward cylinder-dome junctions. Note that this first execution of SUPEROPT produces three different local optimum designs, the “best” (smallest objective) being the one labeled “Local optimum design no. 3”.



**Fig. 9 Vibration modes from GENOPT/BIGBOSOR4 for the optimized propellant tank with two skirts attached to the tank at the aft and forward cylinder-dome junctions.** Compare the GENOPT/BIGBOSOR4 predictions in the top row with predictions from STAGS shown in Figs. 12b. Note that the vibration mode characterized by mostly “rigid body” axial displacement of the tank, analogous to that displayed in Fig. 4(B) in the “oneskirt” case, was never found. It must have a modal vibration frequency that is higher than the 10th eigenvalue for  $n = 0$  circumferential waves, since all of these 10 modes [only the first of which is displayed here in (B)] involve deformation of the domes with little overall extension/compression/shearing of the skirts. Shell deformation modes obtained from STAGS of the type shown in (E), (F) and (G) are not shown in this paper.



**Fig. 10a Prebuckled states, (A), (B) and the critical buckling mode (C) from GENOPT/BIGBOSOR4 for the optimized “twoskirt” propellant tank with skirts attached at the forward and aft cylinder-dome junctions.** From Table 4 and Fig. 8a it is seen that in (A) the stress at Point 1 is fiber tension at the tips of the internal orthogrid stringers (layer 1) in the knuckle of the aft ellipsoidal dome; the stress at Point 2 is fiber compression in layer 1 nodal point 13 of skirt segment 4 (the innermost layer of the laminated composite part of skirt segment 4 where the tapered “prong” thickness is maximum); and the stress at Point 3 is the effective inner surface stress near the thick end of internal prong (node 2, layer 1 of Segment 35) nearest the tank end of the forward skirt. In (B) the stress at Point 1 is fiber tension at the tips of the internal orthogrid stringers in the knuckle of the forward ellipsoidal dome; and the stress at Point 2 is the effective inner fiber stress at the thin end of the internal prong (layer 1 of Segment 4) nearest the tank end of the aft skirt. The stresses listed in this figure are taken from Table 4. Compare with predictions from STAGS shown in Figs. 13a – 13d. (The STAGS models do not show the skirt supports.) (C) shows the critical buckling mode shape and buckling load factors for Load Case 2 (10g lateral acceleration) **corresponding to the prebuckled state along the meridian at the circumferential coordinate, theta = 0 degrees.** In the BIGBOSOR4 model prebuckling in-plane shear, shell wall anisotropy, and transverse shear deformation (t.s.d.) are neglected. In the approximate PANDA-type model [4] prebuckling in-plane shear, shell wall anisotropy and t.s.d. are included in an approximate model in which segment 3 of the conical skirts are modeled as “equivalent” cylindrical shells. **Note that (C) does not show the critical (lowest) buckling load factor under Load Case 2. That critical value, 1.3022, corresponds to shear buckling at theta = 90 degrees, obtained from an approximate PANDA-type model as listed in Table 6.**

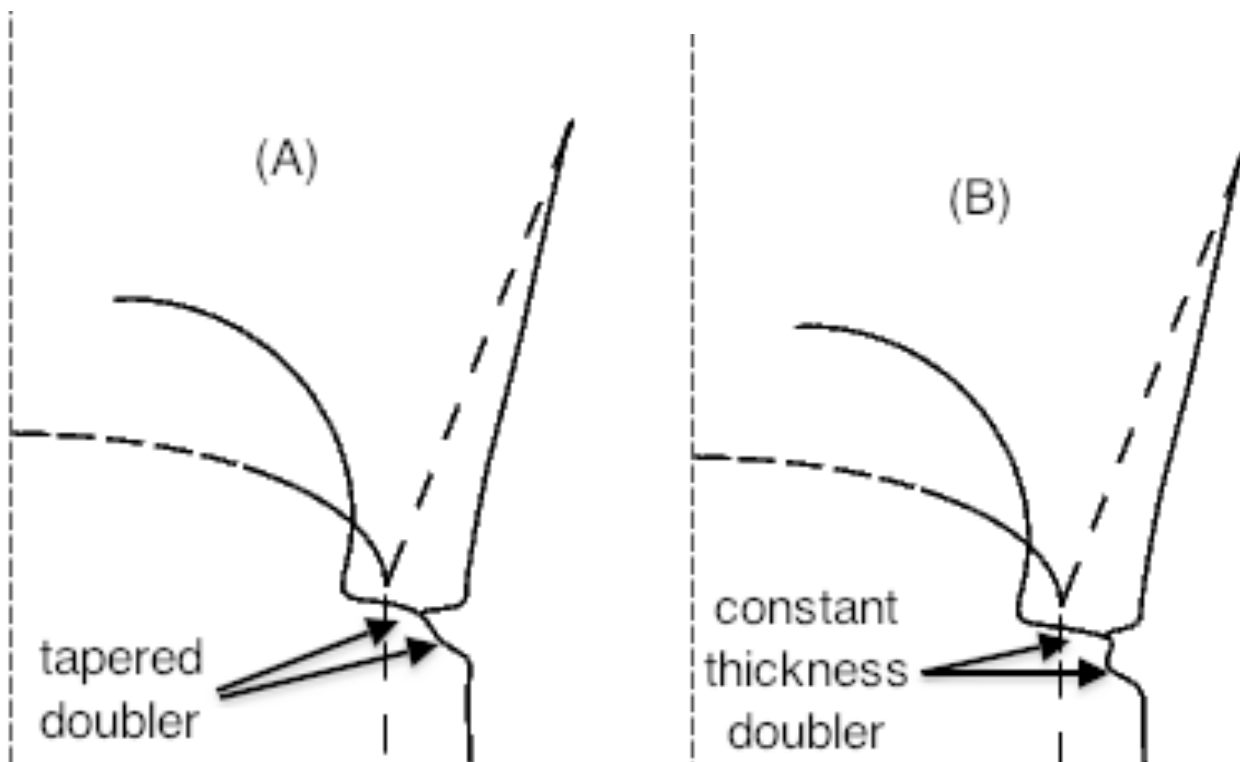


**Fig. 10b Enlarged views of the prebuckled states of the forward part of the optimized “twoskirt” propellant tank as deformed under Load Case 2 (10g lateral acceleration + 25 psi internal pressure + thermal loading) along the meridian at the circumferential coordinate, theta = 0 degrees,** as predicted by two GENOPT/BIGBOSOR4 models. (A) The external doubler, approximately centered at the junction of the forward dome with the cylindrical part of the tank, is double-linearly tapered (as shown in the sketch in Section 1 near the beginning of this paper and in Fig. 1c of [1]) with its maximum thickness, DUBTHK = 0.54 inch, at the dome/cylinder junction, which is also where the forward skirt is joined to the propellant tank. (B) The same overall geometry except that the external doubler has constant thickness over its entire arc width equal to DUBTHK = 0.27 inch, which is equal to the average thickness of the double-linearly tapered doubler. The deformation shown in (A) is the same as that shown in part (B) of the previous figure. The compressive stress at the forward dome/cylinder junction at the tips of the internal orthogrid stringers corresponding to (A) is about -16000 psi. The maximum compressive stress at the same location corresponding to (B) is about -43000 psi. This huge difference in the maximum compressive stress at the tips of the internal orthogrid stringers at the forward dome/cylinder junction is caused by the huge difference in the amount of local meridional bending of the wall of the propellant tank there (approximately midway between the two arrows), evident when the local deformation shown in (A) is compared with that in (B). **The STAGS model corresponds to (B),** and the maximum compressive stress at the tips of the internal orthogrid stringers predicted by the STAGS model is close to -35000 psi, as shown in Fig. 13d. (The -35000 psi is probably not a converged value with respect to finite element mesh density because the blue “contours” in Fig. 13d are very, very thin.) From several executions of BIGBOSOR4 with various model modifications, it was found that neglect of thickness tapering in the two short skirt segments nearest the tank did not significantly affect the maximum compressive stress at the internal orthogrid stringer tips.

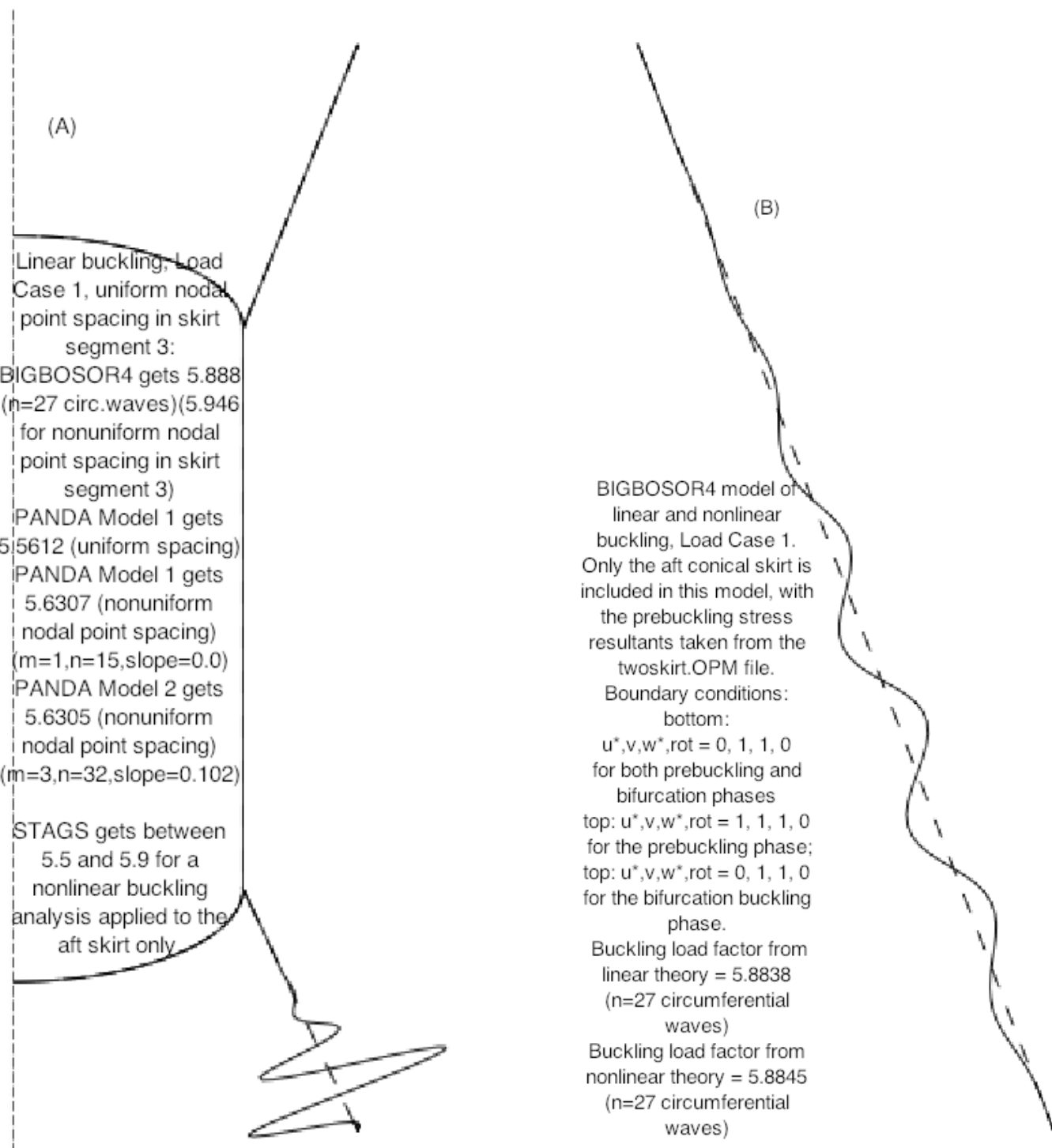
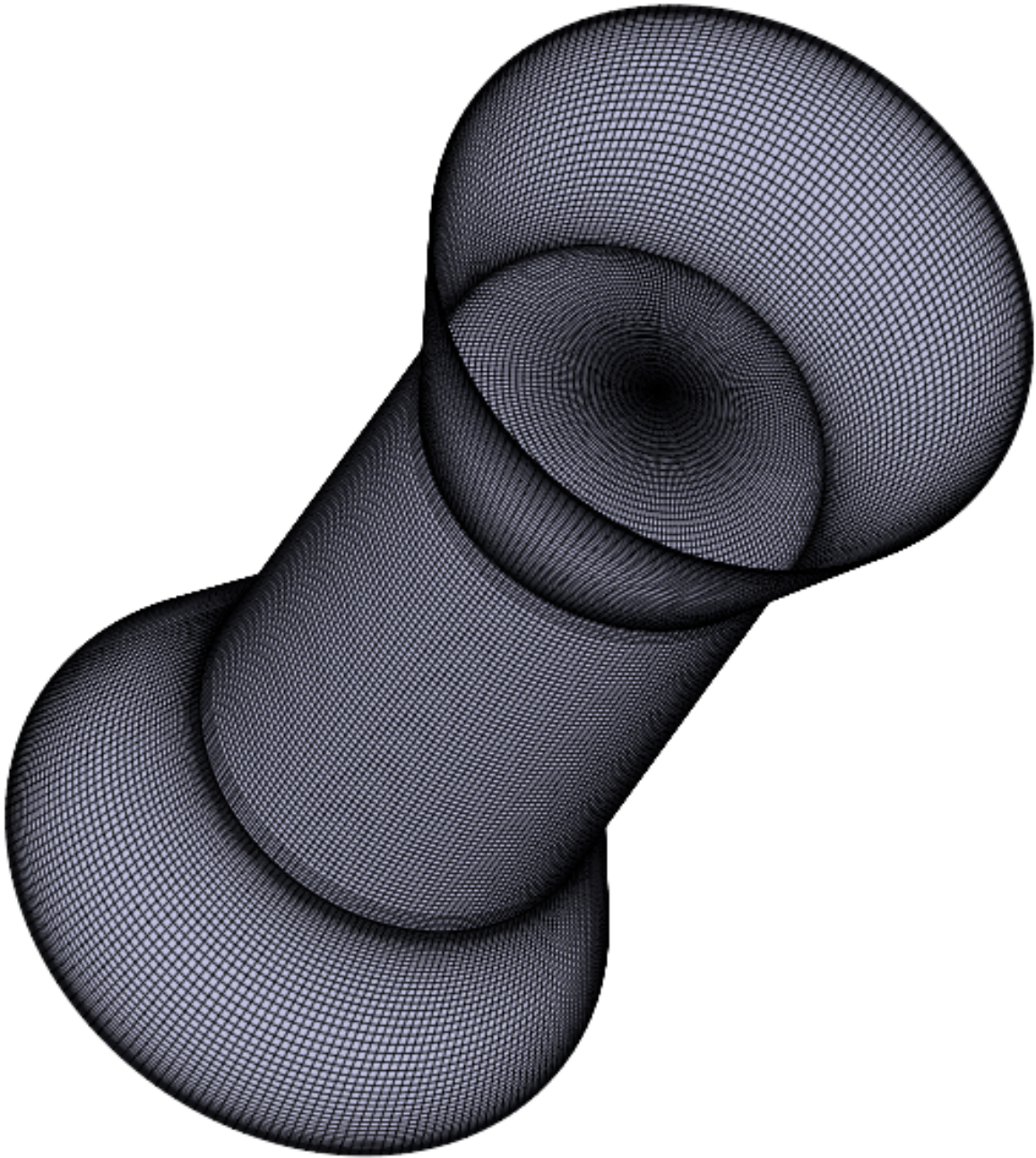
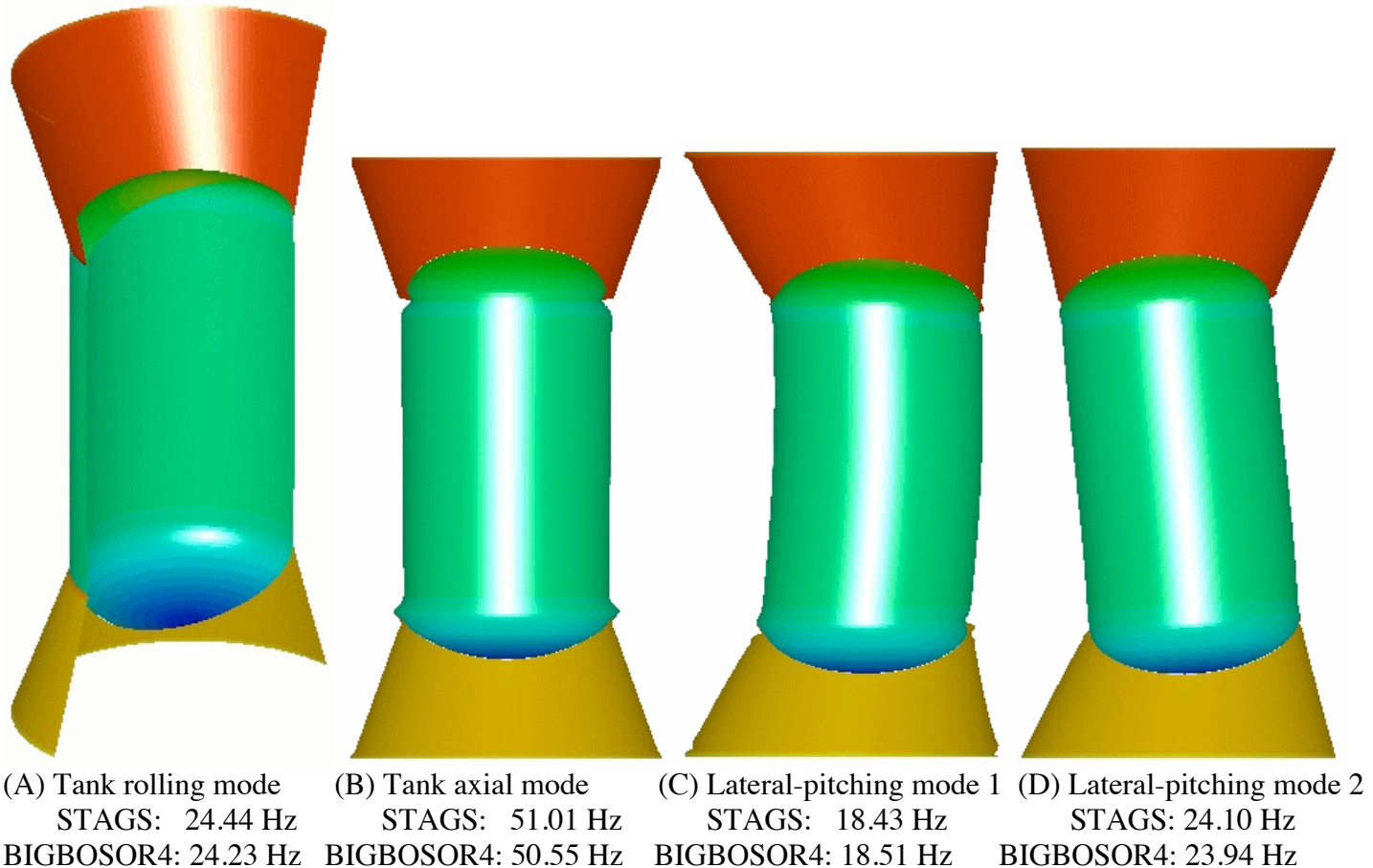


Fig. 11 **BIGBOSOR4 models of buckling of the optimized “twoskirt” configuration under Load Case 1.** (A) the full tank2/skirt system and (B) the aft skirt by itself. In this BIGBOSOR4 model the prebuckling loading is established via the twoskirt.OPM file [2]. Compare these BIGBOSOR4 and PANDA predictions with those from STAGS given in Figs. 14 – 16.



**Fig. 12a STAGS finite element model of the optimized long propellant tank with two conical skirts, aft and forward.** The STAGS “410” finite element is used in the model of the propellant tank shell wall, aft skirt and forward skirt. In this STAGS model the internal orthogrid is represented by a shell wall “layer” with appropriate thickness (thickness equal to the height of the orthogrid stiffeners), material stiffnesses, and density. This is the same strategy as that used to represent the internal orthogrid in the BIGBOSOR4 models.



**Fig. 12b Vibration modes predicted by the STAGS finite element model displayed in the previous figure.**

This is the optimized long propellant tank supported by aft and forward skirts. Compare with the GENOPT/BIGBOSOR4 predictions in the top row of Fig. 9. The predictions listed above labeled “BIGBOSOR4” are from the GENOPT/BIGBOSOR4 software with use of the temporary versions of addbosor4 (addbosor4.tank2.density.var [2]) and bosdec (bosdec.tank2.density.var [2]), not from the “stand-alone” (permanent) version of BIGBOSOR4, which cannot handle material density of a shell wall layer that varies along the meridian within a shell segment. In (B) there appears to be very little tension/compression of the skirts, that is, very little approximately rigid body axial motion of the propellant tank. Instead, the vibration mode in (B) consists mostly of axisymmetric deformation of the end domes with significant local deformation in the neighborhoods of the aft (local outward deformation) and forward (local inward deformation) dome/cylinder junctions. This mode is similar to that predicted by GENOPT/BIGBOSOR4 and displayed in Fig. 9(B).

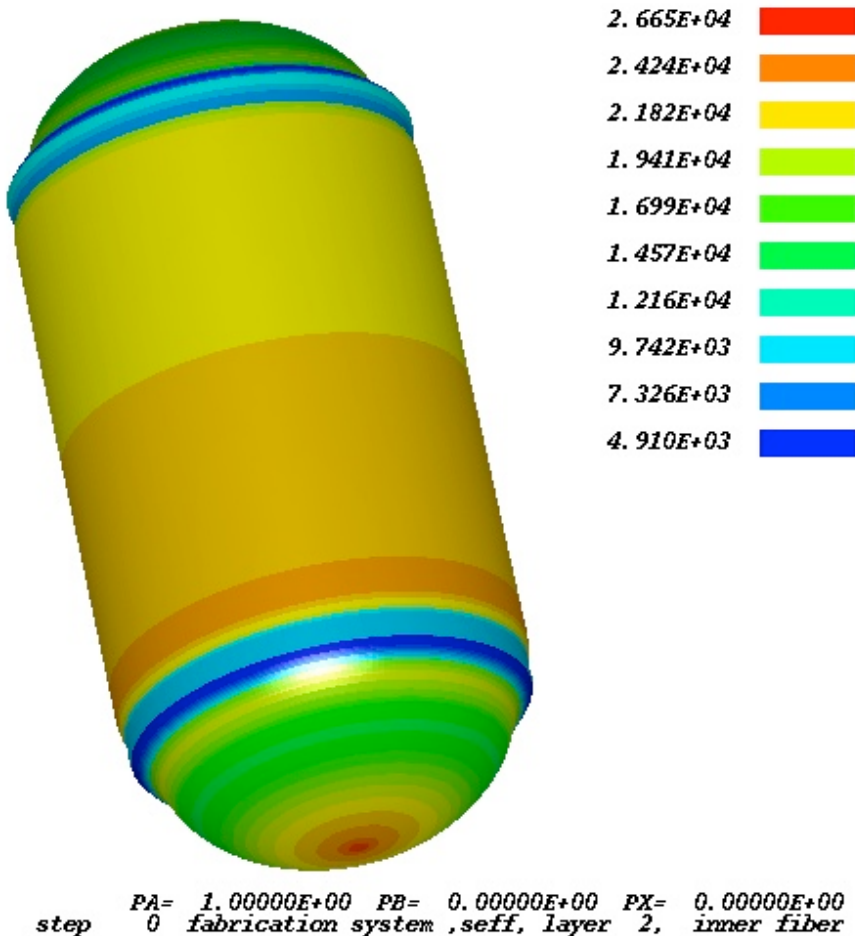


**Fig. 13a Load Case 1 (10g axial acceleration + 25 psi internal pressure + thermal loading): Outer fiber effective stress, “seff” (psi), in the skin of the optimized long propellant tank with aft and forward skirts.** (NOTE: The caption automatically produced by STAGS contains the string, “inner fiber”. In this particular application of STAGS the normal vectors to the shell reference surface all point toward the interior of the tank. Therefore, what STAGS calls “inner fiber” corresponds to the external surface of the tank.) Layer 2 is the skin of the propellant tank to which the internal orthogrid stiffeners are attached. In the STAGS model, Layer 1 represents the internal orthogrid, treated in this paper as an “equivalent” shell wall layer. Hence, the “smeared stiffener” option in STAGS is not used. In the STAGS analysis that produced this figure all the loading is in Load Set A: 10g axial acceleration, 25 psi internal pressure, and 200 degrees tank cool-down. There is no Load Set B. In STAGS jargon the load factor for Load Set A is called “PA” and the load factor for Load Set B is called “PB”. Compare with the GENOPT/BIGBOSOR4 prediction shown in Fig. 10a(A) and in the top part of Table 4. From Table 4, Load Case 1 we have the two entries for maximum stress at the apex of the aft dome (Segment 6 node 2) and at the apex of the forward dome (Segment 33, node 13):

Stress= 2.4268E+04 psi, effect. stress: matl=4 , A , seg=6 , node=2 , layer=2 , z = 0.06 ;FS= 1.50

Stress= 2.3496E+04 psi, effect. stress: matl=7 , A , seg=33, node=13, layer=2, z= 0.04 ;FS= 1.50

Segment 6, node 2 is adjacent to the apex of the aft dome. Segment 33, node 13 corresponds to the apex of the forward dome. The STAGS prediction of effective stress at the aft dome apex, 26650 psi, agrees reasonably well with the GENOPT/BIGBOSOR4 prediction of effective stress at the dome apices.

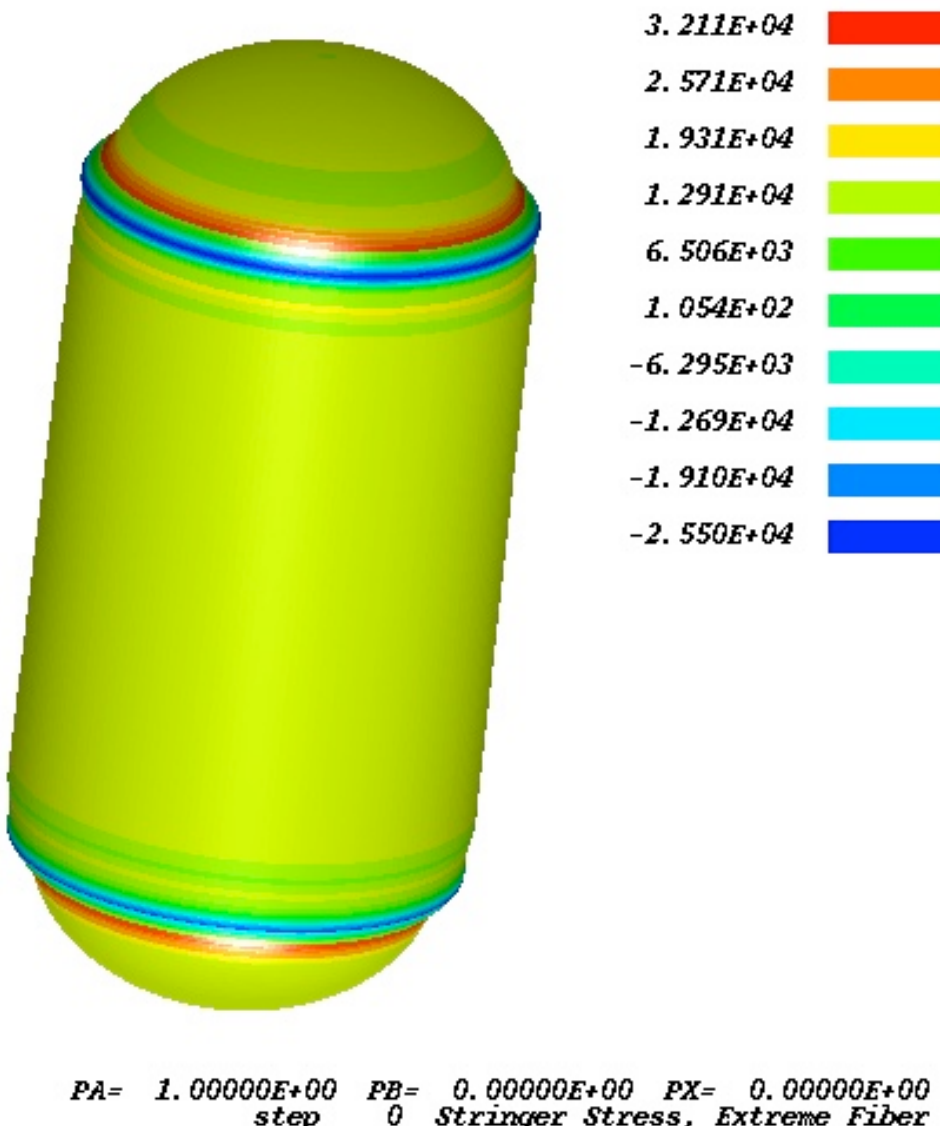
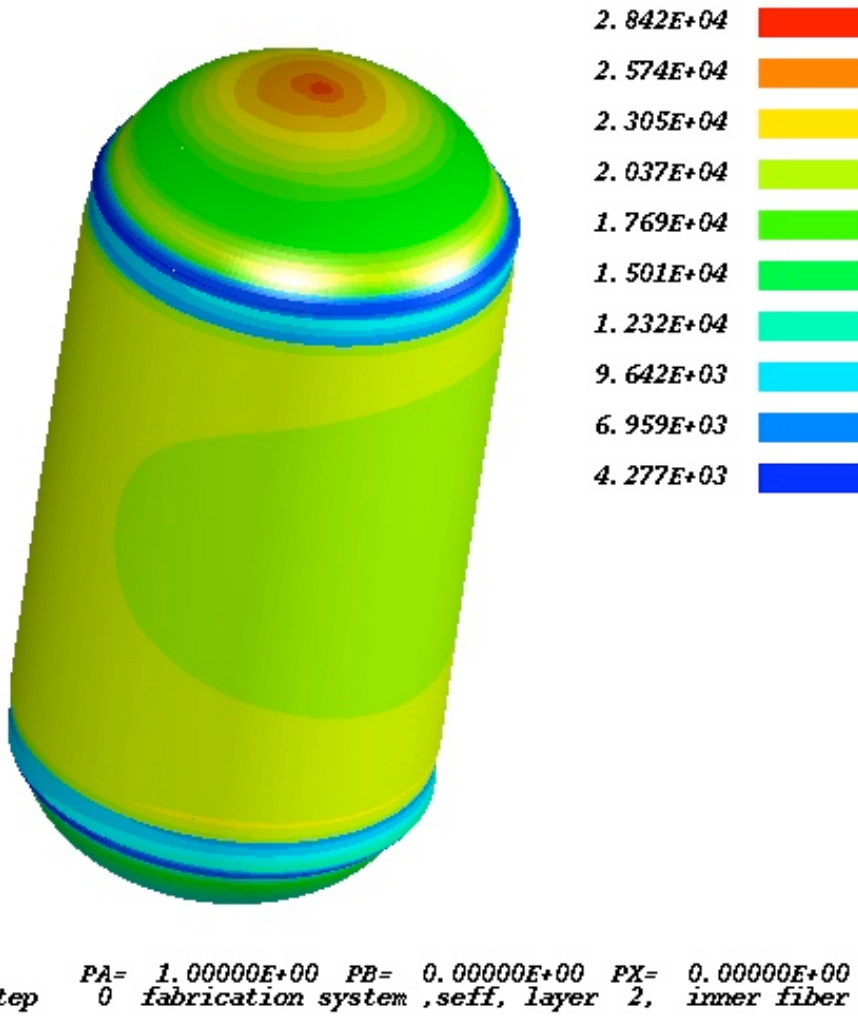


Fig. 13b Load Case 1 (10g axial acceleration + 25 psi internal pressure + thermal loading): STAGS prediction of stress (psi) at the tips of the internal orthogrid stringers. In the STAGS model the internal orthogrid stiffeners are treated as an “effective” shell wall layer with thickness equal to the height of the stiffeners. Hence, the “official smeared stiffener” option in STAGS is not used. The red bands corresponds to the maximum tensile stress at the tips of the internal orthogrid stringers in the knuckle regions of the aft and forward ellipsoidal domes. Compare with the maximum tensile stringer tip stress predicted from the GENOPT/BIGBOSOR4 model at Point 1 indicated in Fig. 10a(A). The forward and aft narrow blue bands correspond to the maximum compressive stress at the orthogrid stringer tips at the junctions between the end domes and the cylindrical part of the propellant tank. In the STAGS model the external doublers that are centered at the dome/cylinder junctions have constant thickness equal to half the maximum thickness of the tapered doublers in the GENOPT/BIGBOSOR4 model. Compare Fig. 10b(A) with Fig. 10b(B) to see the huge difference in maximum compressive stress at the stringer tips predicted from GENOPT/BIGBOSOR4 models with tapered versus constant-thickness doublers. Tapered doublers should be introduced in the STAGS model.



**Fig. 13c Load Case 2 (10 g lateral acceleration + 25 psi internal pressure + thermal loading): Outer fiber effective stress, “seff” (psi), in the skin of the optimized long propellant tank with aft and forward skirts.** (NOTE: The caption automatically produced by STAGS contains the string, “inner fiber”. In this particular application of STAGS the normal vectors to the shell reference surface all point toward the interior of the tank. Therefore, what STAGS calls “inner fiber” corresponds to the external surface of the tank.) In the STAGS analysis that produced this figure all the loading is in Load Set A: 10g lateral acceleration, 25 psi internal pressure, and 200 degrees tank cool-down. There is no Load Set B. In STAGS jargon the load factor for Load Set A is called “PA” and the load factor for Load Set B is called “PB”. Compare with the GENOPT/BIGBOSOR4 prediction shown in Fig. 10a(B) and the bottom part of Table 4. From Table 4, Load Case 2 we have the two entries for maximum stress at the apex of the aft dome (Segment 6 node 2) and at the apex of the forward dome (Segment 33, node 13):

Stress= 1.8883E+04 psi, effect. stress: matl=4 , A , seg=6 , node=2 , layer=2 , z = 0.06 ;FS= 1.50

Stress= 2.6047E+04 psi, effect. stress: matl=7 , A , seg=33, node=13, layer=2, z= 0.04 ; FS= 1.50

Segment 6, node 2 is adjacent to the apex of the aft dome. Segment 33, node 13 corresponds to the apex of the forward dome. The STAGS prediction of effective stress at the dome apex, 28421 psi, agrees reasonably well with the GENOPT/BIGBOSOR4 prediction of effective stress at the forward dome apex.

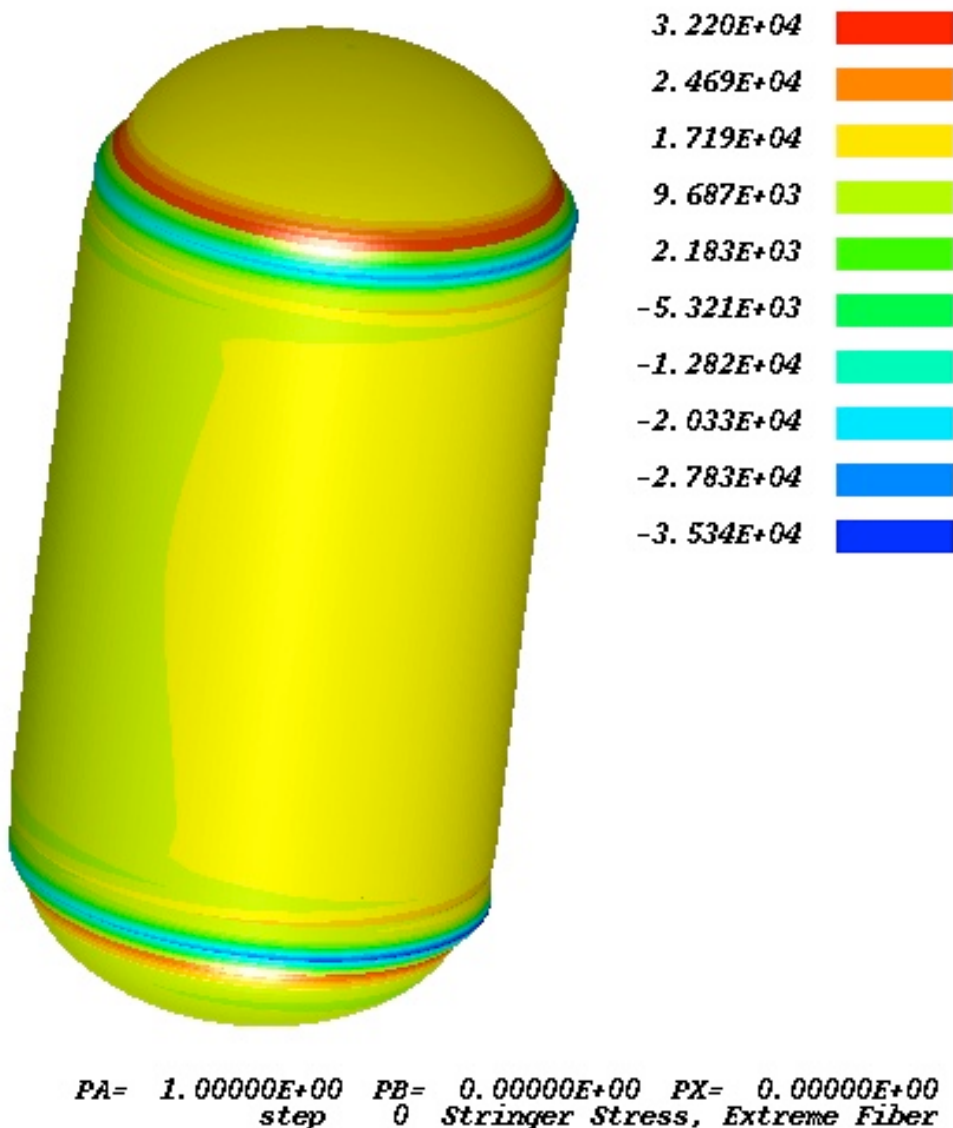


Fig. 13d Load Case 2 (10 g lateral acceleration + 25 psi internal pressure + thermal loading): STAGS prediction of stress (psi) at the tips of the internal orthogrid stringers. In the STAGS model the internal orthogrid stiffeners are treated as an “effective” shell wall layer with thickness equal to the height of the stiffeners. Hence, the “official smeared stiffener” option in STAGS is not used. The red band corresponds to the maximum tensile stress at the tips of the internal orthogrid stringers in the knuckle region of the forward ellipsoidal dome. (There is another similar red band at the knuckle of the aft dome.) Compare with the maximum tensile stringer tip stress predicted from the GENOPT/BIGBOSOR4 model at Point 1 indicated in Fig. 10a(B). The forward and aft very narrow blue bands correspond to the maximum compressive stress at the orthogrid stringer tips at the junctions between the end domes and the cylindrical part of the propellant tank. In the STAGS model the external doublers that are centered at the dome/cylinder junctions have constant thickness equal to half the maximum thickness of the tapered doublers in the GENOPT/BIGBOSOR4 model. Compare Fig. 10b(A) with Fig. 10b(B) to see the huge difference in maximum compressive stress at the stringer tips predicted from GENOPT/BIGBOSOR4 models with tapered versus constant-thickness doublers.

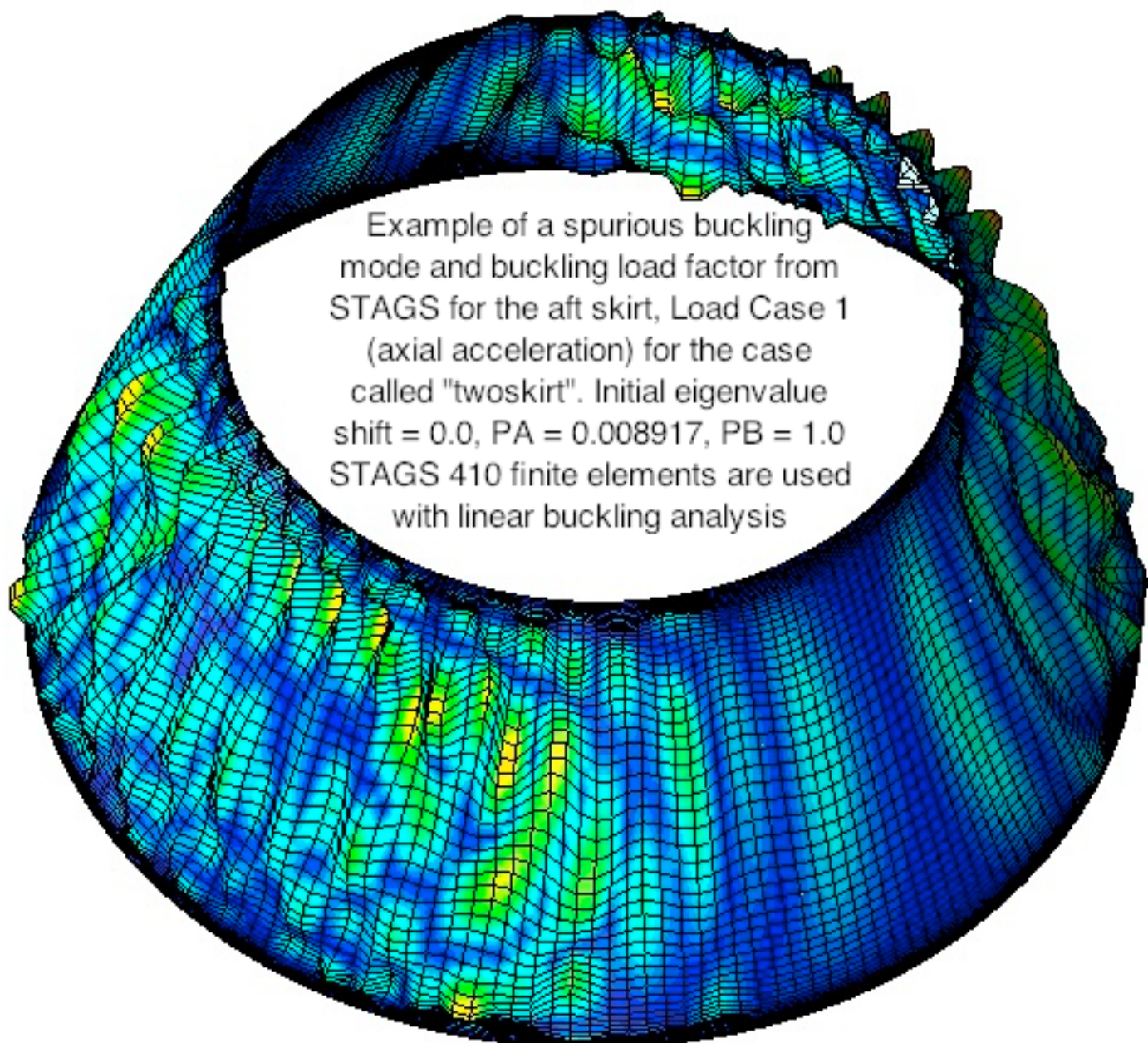
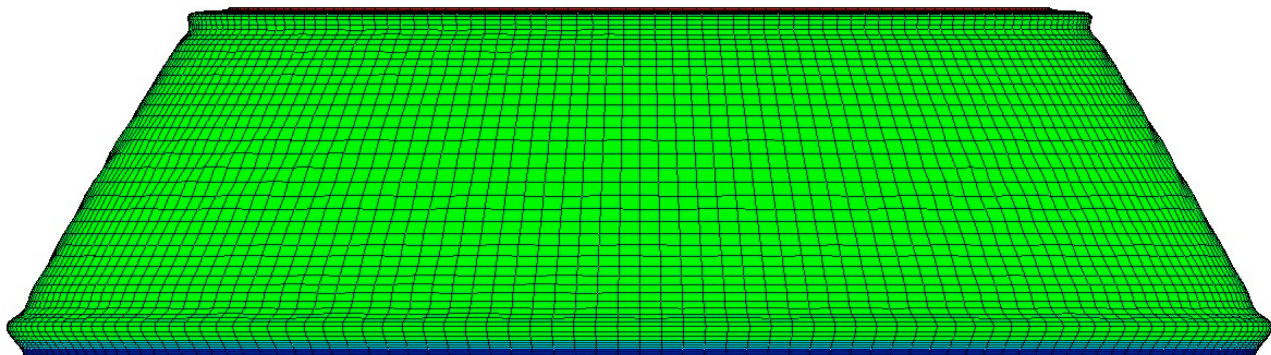
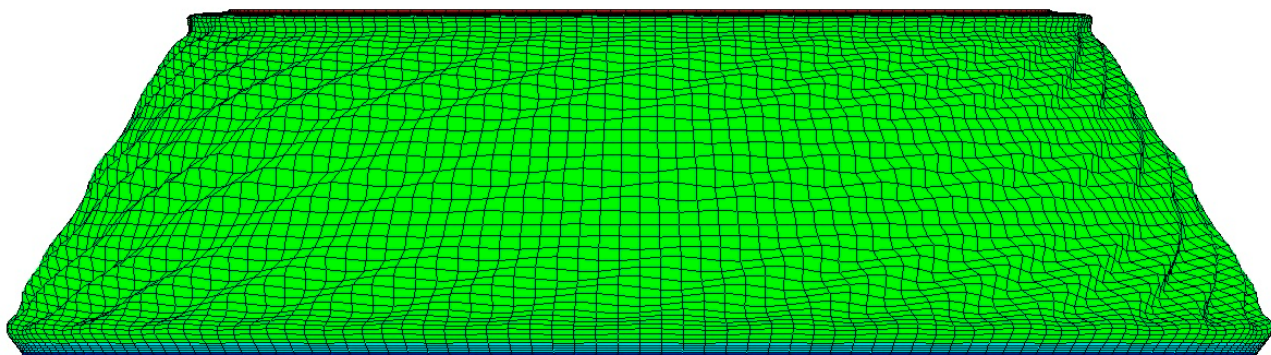


Fig. 14a Optimized “twoskirt” configuration, Load Case 1: STAGS spurious prediction of linear bifurcation buckling of the aft conical support. STAGS could not predict bifurcation buckling from linear theory, either for the entire tank/skirt system or for the aft skirt modeled by itself. It was necessary instead to perform **nonlinear** bifurcation buckling analyses with STAGS in order to obtain predictions that were non-spurious. Results from these nonlinear STAGS models are displayed in the next three figures.



(A) STAGS nonlinear prediction of the state of the "twoskirt" aft conical support at buckling load factor 5.869



(B) STAGS nonlinear prediction of the state of the "twoskirt" aft conical support at buckling load factor 5.9

Fig. 14b Optimized “twoskirt” configuration, Load Case 1: STAGS nonlinear predictions of the state of the aft conical support at a prebuckling load near (A) incipient non-axisymmetric buckling, load factor, PA = 5.869, and (B) at a slightly higher load factor, PA = 5.9. The load factor for load set B remains at PB=1.0 throughout. The predictions from STAGS for buckling under Load Case 1 are in good agreement with those from BIGBOSOR4 and PANDA shown and listed in Fig. 11.

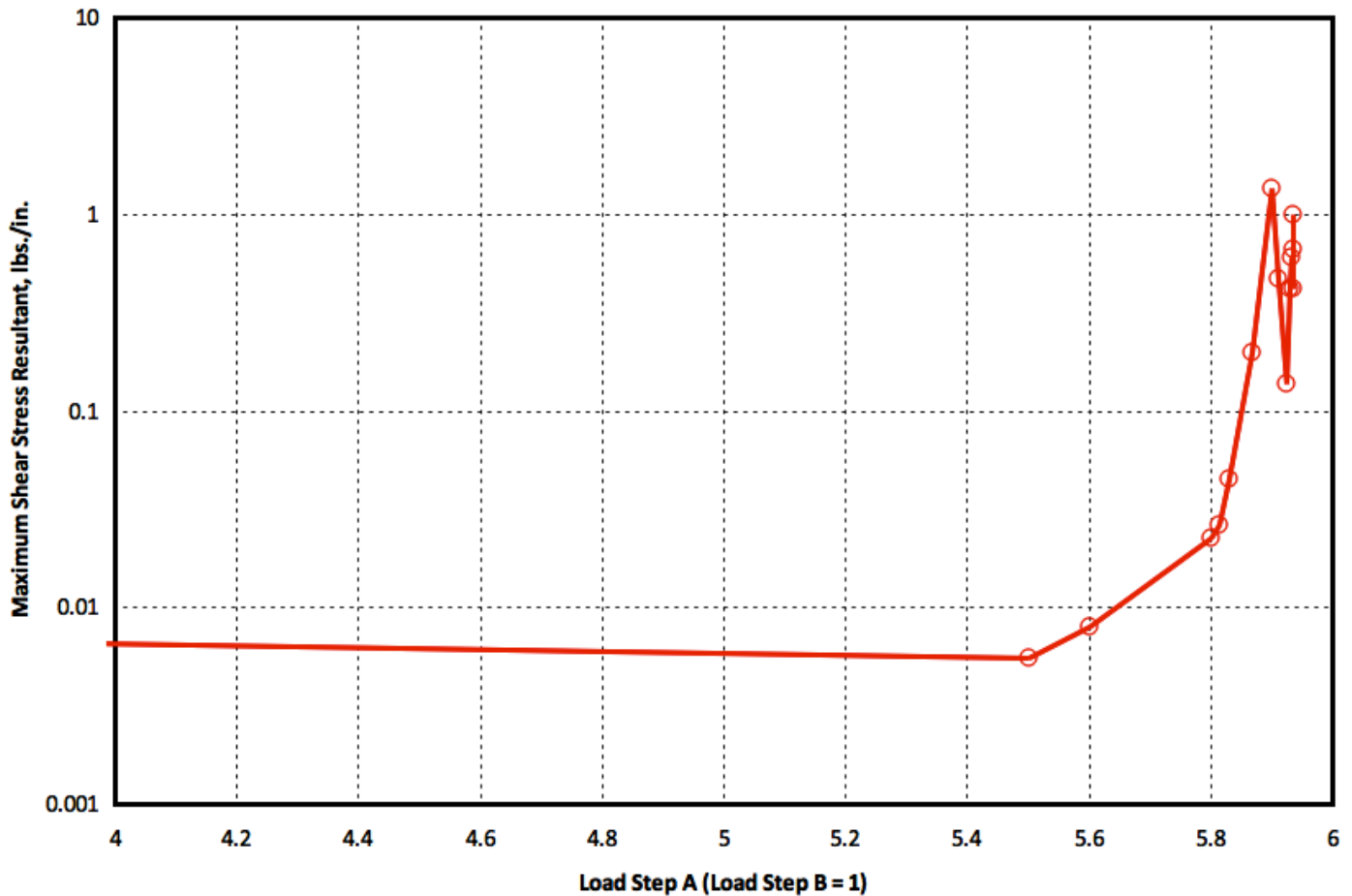
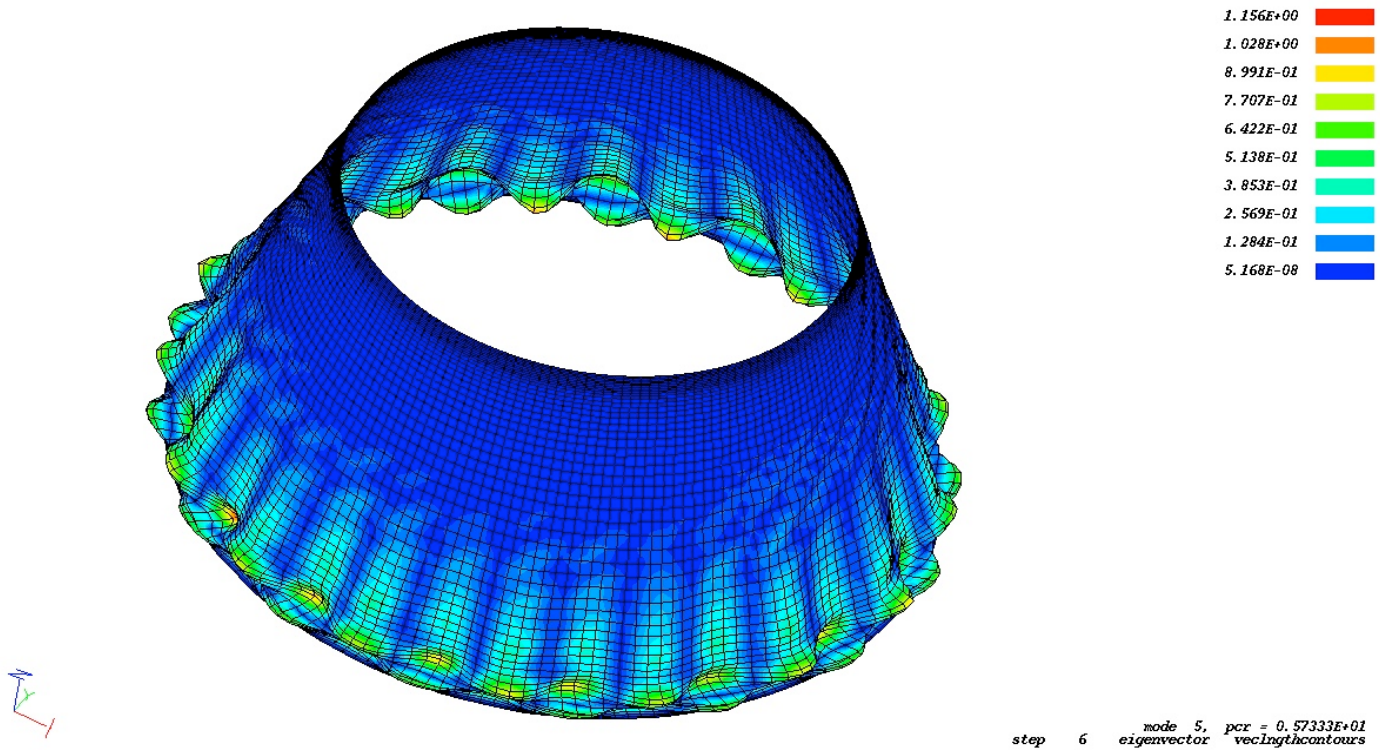


Fig. 15 Optimized “twoskirt” configuration, Load Case 1: STAGS nonlinear prediction of the maximum shear stress resultant (lb/in) in the aft skirt as a function of Load Step A (load factor, PA, in STAGS jargon). From this figure it appears that incipient buckling of the aft skirt may be present at a load factor as low as 5.5. This prediction is in good agreement with the GENOPT/skirt prediction of 5.5612 from the PANDA-type model [4] as listed in the plot on the left-hand side of Fig. 11.



**Fig. 16 Optimized “twoskirt” configuration, Load Case 1: STAGS prediction of nonlinear bifurcation buckling of the aft conical support. The nonlinear bifurcation buckling load factor is 5.7333.** This nonlinear load factor from STAGS and the bifurcation buckling mode shape are in reasonably good agreement with those from the approximate PANDA-type **Model 2** listed near the end of Table 5: PANDA-type **Model 2** buckling load factor = 5.6305 with MSKIN = 3 meridional half waves over the lowest 1/4 of the **aft** conical skirt, NSKIN = 32 circumferential half waves over 180 degrees of the circumference, and slope, SLOPE, of the buckling nodal lines of 0.10167. PANDA-type **Model 2** includes only the lowest 1/4th of the **aft** conical skirt (nearest the large-diameter end). As listed in Table 5, in this PANDA-type **Model 2** the hoop resultant, NYAVE, and in-plane shear resultant, NXYAVE, are set to zero, the meridional resultant from Load Set A (eigenvalue load), NXAVE = -247.87 lb/in, and the meridional resultant from Load Set B (fixed load), NXFIX = 1223.5 lb/in. In the PANDA-type **Model 2** the lowest 1/4 of the **aft** conical skirt is modeled as an “equivalent” simply supported cylindrical shell with length, FLEFF = 34.821 inches and radius, RAVE = 160.71 inches. The stress resultants from Load Set A (NXAVE = N1VAR = -247.87 lb/in) and Load Set B (NXFIX = N1FIX = 1223.5 lb/in) are those corresponding to nodal point no. 10 in Segment 3 of the **aft** skirt, as listed in the section of the twoskirt.OPM file [2] pertaining to Load Case 1 and the prebuckling response of the **aft** conical skirt at circumferential coordinate, theta = 0 degrees. This list of the prebuckling response in the twoskirt.OPM file contains the following lines:

```

PREBUCKLING STRESS RESULTANTS IN THE SKIRT(1), THETA= 0.0000E+00
NODE MERIDIONAL RESULTANT CIRCUMFER. RESULTANT IN-PLANE SHEAR
J      N1VAR          N2VAR          N12VAR        N1FIX          N2FIX
10     -2.4787E+02    -1.0030E-01    0.0000E+00    1.2235E+03   -1.8839E+01

```

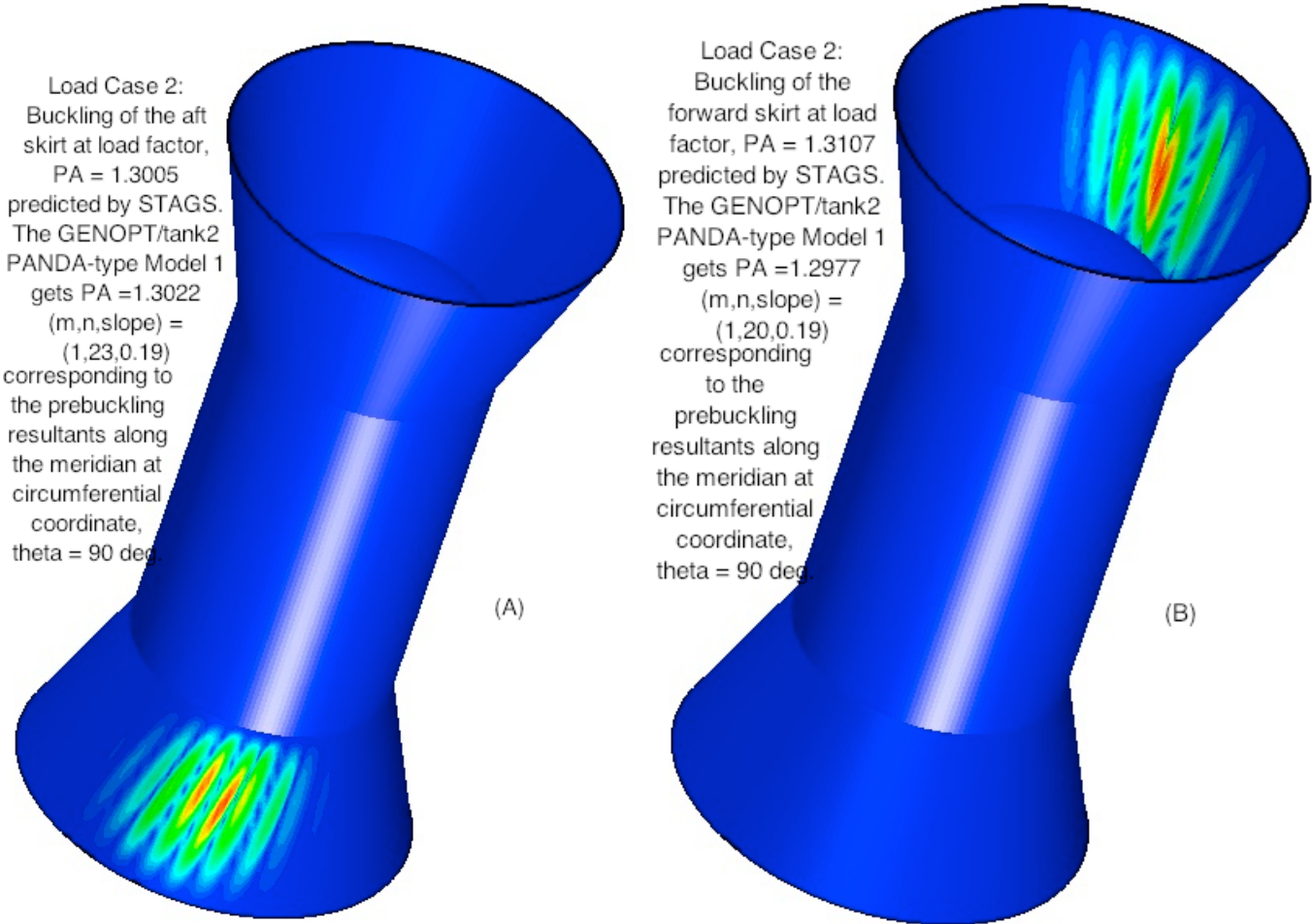


**Fig. 17 Optimized “twoskirt” configuration, Load Case 2: STAGS prediction of nonlinear bifurcation buckling of (A) the aft skirt and (B) the forward skirt from a finite element model that includes the entire tank/skirt system.** The predictions from STAGS are in excellent agreement with those from the PANDA-type predictions [4]. The ingredients of the PANDA-type **Model 1** prediction for buckling of the **aft skirt** at circumferential coordinate, **theta = 90 degrees**, are listed in Table 6. The ingredients of the PANDA-type prediction for buckling of the forward skirt at theta = 90 degrees are similar. In the PANDA-type **Model 1** the conical skirts are modeled as “equivalent” cylindrical shells. For example, from Table 6 we see that the aft conical skirt is modeled as an equivalent cylindrical shell with length, FLEFF = 139.28 inches, and radius, RAVE = 133.93 inches. The uniform prebuckling resultants in the aft skirt at theta = 90 degrees are as follows:

Load Set A: (“eigenvalue” loads): NXAVE = -22.837 lb/in, NYAVE = -0.0000015, NXAVE = 253.61 lb/in

Load Set B: (“fixed” loads): NXFIX = +1432.6 lb/in, NYFIX = +0.62338 lb/in, NXYFIX = 0.00 lb/in

#### The critical buckling mode of the aft skirt from the approximate PANDA-type Model 1:

Number of axial half waves over the effective length, FLEFF = MSKIN = 1,

Number of circumferential half waves over 180 degrees of the circumference = NSKIN = 23,

Slope of the buckling nodal lines = 0.19008.

The “equivalent” cylindrical shell of the PANDA-type **Model 1** of the **forward skirt**, its loading at theta = 90 degrees, and its critical buckling mode and load factor are analogous to those of the aft skirt.